



The memory of neuronal mitochondrial stress is inherited transgenerationally via elevated mitochondrial DNA levels

Qian Zhang^{1,2}, Zihao Wang^{1,2}, Wenfeng Zhang^{1,2}, Qingbo Wen^{1,2}, Xinyu Li^{1,2}, Jun Zhou^{1,2},
Xueying Wu¹, Yongqing Guo^{1,2}, Yangli Liu¹, Changshuo Wei^{2,3}, Wenfeng Qian^{1,2,3} and Ye Tian^{1,2,4}✉

The memory of stresses experienced by parents can be passed on to descendants as a forecast of the challenges to come. Here, we discovered that the neuronal mitochondrial perturbation-induced systemic mitochondrial unfolded protein response (UPR^{mt}) in *Caenorhabditis elegans* can be transmitted to offspring over multiple generations. The transgenerational activation of UPR^{mt} is mediated by maternal inheritance of elevated levels of mitochondrial DNA (mtDNA), which causes the proteostasis stress within mitochondria. Furthermore, results from intercrossing studies using wild *C. elegans* strains further support that maternal inheritance of higher levels of mtDNA can induce the UPR^{mt} in descendants. The mitokine Wnt signalling pathway is required for the transmission of elevated mtDNA levels across generations, thereby conferring lifespan extension and stress resistance to offspring. Collectively, our results reveal that the nervous system can transmit stress signals across generations by increasing mtDNA in the germline, enabling descendants to better cope with anticipated challenges.

Environmental factors and physiological stresses can lead to changes in traits and behaviours in various organisms across multiple generations, and the identified molecular mechanisms underlying these outcomes include epigenetic regulation as well as other forms of inheritance (for example, maternal effects on oocyte provisioning)^{1–8}. Notably, germline reprogramming of epigenetic marks typically limits the propagation of such effects to only a few successive generations. However, the memory of other stresses, such as those sensed by mitochondria—organelles that are directly inherited maternally through oocytes—might also exhibit transgenerational inheritance^{3,9–13}. Mitochondria have their own genome (mtDNA), which encodes 13 proteins in mammals (12 in *C. elegans*) that are part of the mitochondrial oxidative phosphorylation (OXPHOS) and ATP synthase complexes¹⁴. The rest of the proteins that function in mitochondria are encoded by the nuclear genome (nDNA). The interplay between the mitochondrial and nuclear genomes is especially evident for the large OXPHOS complexes, which consist of protein subunits encoded by both genomes. Stress conditions are known to trigger an imbalance between the production and assembly of proteins encoded by both mtDNA and nDNA, and such disruption of proteome homeostasis within mitochondria quickly triggers a specific transcriptional response that is known as the UPR^{mt} (refs. ^{15–17}).

The UPR^{mt} is typically induced in a cell-autonomous manner^{18–23}. However, recent research demonstrated that UPR^{mt} signals can also be communicated through intercellular signalling across multiple tissues^{24–31}. For example, the expression of the Huntington's disease-causing protein (Q40) or the reduction of *cco-1* (complex IV subunit of electron transport chain) expression in neurons results in a UPR^{mt} response in peripheral tissues of *C. elegans*^{24,25}. The cell non-autonomous induction of the UPR^{mt} enables a global

stress response that prepares the organism to better cope with local mitochondrial stress²⁵. This discovery prompted the proposal of a mechanistic hypothesis in which a factor, termed the mitokine, is generated in neurons and then secreted and subsequently perceived by the peripheral tissues, where it induces the UPR^{mt} (ref. ²⁴). Our previous study identified the Wnt ligand/EGL-20 as the mitokine signal that coordinates the mitochondrial stress response between the nervous system and the intestine³².

In this Article, we describe the serendipitous observation that the systemic UPR^{mt} triggered by neuronal mitochondrial stresses can be transmitted for multiple generations, even a long time after the original stress signal has been removed. This transgenerational induction of UPR^{mt} was caused by the inheritance of increased levels of mtDNA, which lead to a mitonuclear imbalance, thereby generating stressed mitochondria in each generation. The mitokine Wnt signalling enables the propagation and maintenance of increased mtDNA levels across generations, thereby conferring lifespan extension and stress resistance to offspring with a trade-off in fitness.

Results

Neuronal mitochondrial stress triggers the transgenerational induction of UPR^{mt}. Neuronally expressed Huntington's disease-causing protein Q40 fused with yellow fluorescent protein (neuronal Q40::YFP) physically interacts with mitochondria and affects mitochondrial function, eliciting a systemic UPR^{mt} in *C. elegans*, as demonstrated by the induction of the mitochondrial chaperone reporter *hsp-6p::gfp*^{25,32} (Fig. 1a,b). When these animals were analysed using crossing experiments, we were surprised to observe that ~30% of genetically wild-type (WT) F₁ descendants generated from P₀ hermaphrodites (the progeny of crosses between neuronal *rgef-1p::Q40::yfp; hsp-6p::gfp* hermaphrodites (herm) and

¹State Key Laboratory of Molecular Developmental Biology, Institute of Genetics and Developmental Biology, Chinese Academy of Sciences, Beijing, China.

²University of Chinese Academy of Sciences, Beijing, China. ³State Key Laboratory of Plant Genomics, Institute of Genetics and Developmental Biology, Innovation Academy for Seed Design, Chinese Academy of Sciences, Beijing, China. ⁴Center for Excellence in Animal Evolution and Genetics, Chinese Academy of Sciences, Kunming, China. ✉e-mail: ytian@genetics.ac.cn

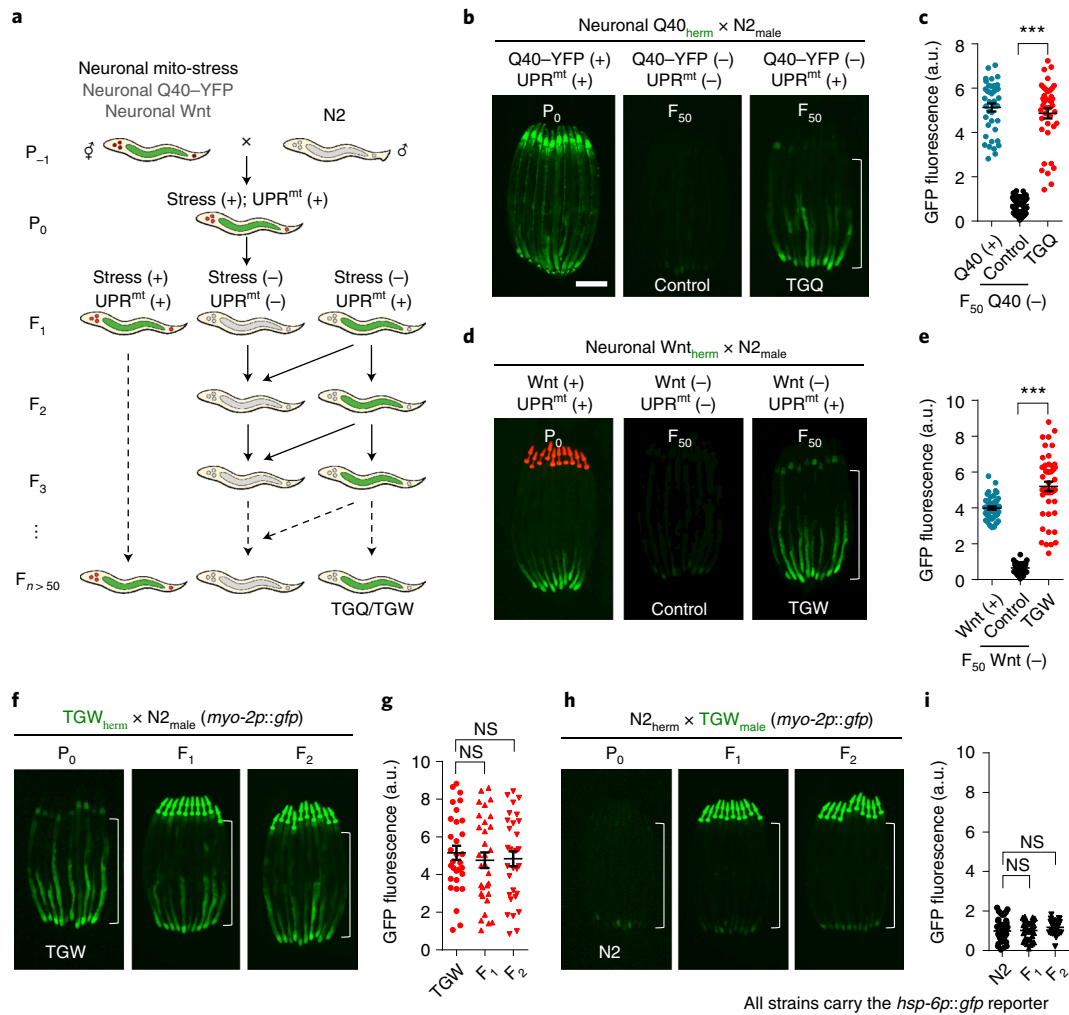


Fig. 1 | Neuronal mitochondrial perturbations transmit the systemic UPR^{mt} across multiple generations. **a**, Schematic of the strategy used to generate animals exhibiting the transgenerational UPR^{mt}. The hermaphrodites (P_{-1}) exhibiting the induction of the UPR^{mt} in response to the neuronal mitochondrial stresses (for example, neuronal Q40::YFP, neuronal Wnt/EGL-20) were crossed with WT males to generate hermaphrodites (P_0), and these P_0 animals were then self-crossed to generate F_1 animals with different genotypes. The F_1 animals without the original stress but that still exhibited the induction of the UPR^{mt} were maintained as animals with transgenerational induction of the UPR^{mt}. Further detailed information is provided in Extended Data Fig. 1. **b–d**, Fluorescence visualization of the *hsp-6p:gfp* reporter in animals (F_{50}) with or without expression of either neuronal Q40-YFP (**b**) or neuronal Wnt (**d**). Animals exhibiting the transgenerational UPR^{mt} generated from the neuronal Q40-YFP or neuronal Wnt expression were referred to as TGQ or TGW, respectively. The region in which *hsp-6p:gfp* is induced is highlighted. Scale bar, 250 μ m, also applies to **d**, **f** and **h**. **e, f**, Quantification of the *hsp-6p:gfp* reporter as described in **b** and **d**, respectively. $n = 40$ (Q40 (+)), $n = 50$ (control; **c**), $n = 40$ (TGQ), $n = 47$ (Wnt (+)), $n = 42$ (control; **e**) and $n = 47$ (TGW) worms. **g, h**, Fluorescence visualization (**f**) and quantification (**g**) of the *hsp-6p:gfp* reporter in TGW hermaphrodites (P_0), and the progeny generated from the cross between the TGW hermaphrodites (P_0) and the WT males (labelled with pharyngeal muscle reporter *myo-2p:gfp*). Both F_1 (cross-progeny) and F_2 (self-cross) animals exhibited the induction of UPR^{mt}. $n = 31$ worms. **i**, Fluorescence visualization (**h**) and quantification (**i**) of the *hsp-6p:gfp* reporter in WT hermaphrodite (P_0), and the progeny generated from the cross between the TGW males (labelled with the *myo-2p:gfp* reporter) and the WT hermaphrodite (P_0). $n = 47$ (N2), $n = 34$ (F_1) and $n = 37$ (F_2) worms. Data are mean \pm s.e.m. P values were determined using two-sided Student's *t*-tests; *** $P < 0.001$; NS, $P > 0.05$. The exact P values are provided as source data. Source data are available online.

hsp-6p:gfp males) maintained the UPR^{mt} even though the neuronal *rgef-1p::Q40::yfp* transgene had been crossed out (Fig. 1a and Extended Data Fig. 1). When following up on these individual F_1 WT animals with strong *hsp-6p:gfp* expression, we found that approximately ~80% of them passed on the UPR^{mt} signal to their self-fertilized progeny with a penetrance of 40–60% (Fig. 1a and Extended Data Fig. 1). As we continued following the descendants of these F_1 animals that maintained strong *hsp-6p:gfp* expression, the transmission efficiency for certain animals gradually increased to 70–90% by the F_2 generation, whereas others gradually lost the UPR^{mt} signal in later generations without selection for strong

hsp-6p:gfp expression (Fig. 1a and Extended Data Fig. 1). We repeatedly observed that the UPR^{mt} triggered by neuronal Q40-YFP was transmitted over more than 50 generations in multiple independent lines (Fig. 1a–c and Extended Data Figs. 1 and 2). We refer to these genetically WT animals exhibiting strong UPR^{mt} as transgenerational effect of neuronal Q40 (TGQ) animals (Fig. 1a–c).

As we previously demonstrated that Wnt/EGL-20 signalling is required and sufficient to propagate the UPR^{mt} signal from the nervous system to peripheral tissues³², we next investigated whether neuronal Wnt signalling alone was sufficient to pass on the UPR^{mt} to the next generation. Similarly, we found that the systemic UPR^{mt}

triggered by neuronal EGL-20 could also be transmitted over more than 50 generations (Fig. 1a,d,e and Extended Data Fig. 1). Moreover, the transgenerational UPR^{mt} was not due to the transmission of exogenous expression of *egl-20* from parents to offspring (Extended Data Fig. 2a). We refer to these genetically WT animals exhibiting the UPR^{mt} triggered by neuronal Wnt as transgenerational effect of neuronal Wnt signalling (TGW) animals.

To determine whether other types of mitochondrial stress could also trigger the transgenerational UPR^{mt}, we examined the expression of *hsp-6p::gfp* in the descendants of animals with various mitochondrial perturbations. The UPR^{mt} triggered by neuronal *cco-1* knockdown could also induce the UPR^{mt} transgenerationally with a lower penetrance (Extended Data Fig. 2b). By contrast, whole-worm RNA interference (RNAi) against the mitochondrial OXPHOS genes *cco-1* and *atp-3* (neurons are insensitive to RNAi provided through conventional feeding treatment) and drug treatments disrupting parental mitochondrial functions were not able to trigger the transgenerational UPR^{mt} in descendant animals (F₂) (Extended Data Fig. 2c-g). The cellular stresses that the nervous system can sense and communicate to peripheral tissues are not restricted to mitochondria. Neuronal expression of *xbp-1s* is sufficient to induce the endoplasmic reticulum unfolded protein response (UPR^{ER}) in distal intestinal cells in *C. elegans*³³. However, we did not observe the UPR^{ER} in the descendants of animals with neuronal expression of *xbp-1s* (Extended Data Fig. 2h). Collectively, our results show that neuronal mitochondrial perturbations can cause the transmission of the systemic UPR^{mt} to offspring across multiple generations in *C. elegans*.

The transgenerational UPR^{mt} is inherited maternally. As mitochondria are normally exclusively inherited from the mother, we next tested whether the transgenerational UPR^{mt} was also transmitted maternally. We crossed TGW hermaphrodites with WT males, and found that both F₁ (cross-progeny) and F₂ (self-cross) animals exhibited the UPR^{mt} with a penetrance of 70%–90%, which is similar to the penetrance observed for P₀ TGW hermaphrodite animals (Fig. 1f,g). By contrast, when TGW males were crossed with WT hermaphrodites, none of the F₁ (cross-progeny) or F₂ (self-cross) animals exhibited the UPR^{mt} (Fig. 1h,i). Conspicuously, the transgenerational UPR^{mt} phenotype did not segregate with a Mendelian ratio; rather, it was invariably maternally inherited with incomplete penetrance.

Note that mtDNA mutations, which are maternally inherited, can also lead to the induction of the UPR^{mt}; we therefore sequenced the mitochondrial genomes of the animals used in our study. All parental strains carry four mutations compared with the N2 reference sequence—one synonymous and three non-synonymous mutations—suggesting that these strains were derived from the reference N2 but accumulated mutations as they were bred in the laboratory. Nonetheless, these four mutations have been fixed (100% in frequency) and no additional variation in the mtDNA sequence was detected among the F₅ descendant progeny with or without UPR^{mt} induction (four lines) (Extended Data Fig. 3 and Supplementary Table 3). Thus, these results rule out the possibility that the observed transgenerational UPR^{mt} could have resulted from selection pressure favouring pre-existing deleterious mtDNA mutations. It is also worth mentioning that, in all of our genetic studies, we invariably maintained several worms in each generation to avoid the accumulation and fast genetic drift of any random de novo mutations.

Descendants with transgenerational UPR^{mt} carry elevated levels of mtDNA. To examine the mechanism that underlies the transgenerational UPR^{mt}, we performed RNA sequencing (RNA-seq) analyses. Comparative analysis of TGQ versus unaffected WT worms identified 1,836 differentially expressed genes (fold change ≥ 2 , adjusted $P \leq 0.05$) (Supplementary Table 4). Gene Ontology-KEGG

pathway analysis showed enrichment of differentially expressed genes in the mtDNA-encoded OXPHOS pathway and the Wnt signalling pathway (Fig. 2a and Supplementary Table 4). We noticed that the most significantly upregulated OXPHOS genes were encoded by the mitochondrial genome (Fig. 2b). Quantitative PCR (qPCR) analyses showed that the transcripts of mtDNA-encoded OXPHOS and ATP synthase genes were significantly upregulated in both TGQ and TGW animals, whereas nDNA-encoded genes were only slightly or not significantly changed in TGQ or TGW animals (Fig. 2c and Extended Data Fig. 4a). Moreover, the expression of mitochondrial chaperones (*hsp-6* and *hsp-60*) and mtDNA polymerase gamma *polg-1* was significantly upregulated in both TGW and TGQ animals; however, the expression of genes (*hmg-5*, *rpom-1* and *tfbm-1*) involved in the transcriptional regulation of mtDNA was not significantly changed (Fig. 2d and Extended Data Fig. 4b).

Thus, we measured the mtDNA levels of TGW and TGQ animals by first assessing the mtDNA/nDNA ratio³⁴. The mtDNA levels in *C. elegans* remained constant before the L3 stage, followed by an initial increase at the L4 stage and then significant increases associated with germline development³⁵ (Extended Data Fig. 4c). Indeed, we found that TGW animals had significantly higher relative mtDNA levels compared with unaffected WT animals at the L1, L4 and adult stages (Fig. 2e and Extended Data Fig. 4d,e). Similarly, an increase in relative mtDNA levels was also observed in TGQ and transgenerational UPR^{mt} triggered by neuronal *cco-1* knockdown (TGCK) animals (Extended Data Fig. 4f). Both TGW and TGQ animals carried $\sim 1.7 \times 10^5$ copies of mtDNA at the early L4 stage, whereas unaffected WT animals carried $\sim 1.3 \times 10^5$ copies of mtDNA (Fig. 2f and Extended Data Fig. 4g). Furthermore, the relative mtDNA levels in dissected gonads and the mtDNA copy numbers in isolated oocytes were significantly higher in both parental and TGW animals compared with in WT animals (Fig. 2g,h and Extended Data Fig. 4h,i), and the transcript levels of *hsp-6* were also significantly higher in the dissected gonads of TGW worms compared with the transcript levels in WT animals (Extended Data Fig. 4j).

Notably, the ratios of mtDNA/nDNA were variable among individual TGW animals (Extended Data Fig. 4d). We therefore grouped the TGW animals into two populations according to their *hsp-6p::gfp* signal intensity (weak TGW and strong TGW). Closer examination of these two groups revealed two conspicuous differences. First, the *hsp-6p::gfp* expression levels in weak TGW animals gradually diminished and returned to the basal level in about three generations (Extended Data Fig. 4k). Second, the relative mtDNA level of the strong TGW animals was significantly higher compared with the level of the weak TGW animals (Fig. 2i).

To monitor how elevated mtDNA levels were propagated across generations in TGW animals, we quantified the relative mtDNA levels at the single-worm level in populations with/without neuronal mitochondrial stress and with/without selection of UPR^{mt} from the F₂ to F₂₀ generation. We consistently found that TGW animals had significantly higher mtDNA/nDNA ratios than their unaffected siblings (without stress; without selection for the UPR^{mt}) in each generation (Fig. 2j). Although the unaffected siblings also exhibited increased mtDNA/nDNA ratios at the F₂ and F₃ generations, the higher levels of mtDNA gradually decreased to normal levels in later generations if selection for strong UPR^{mt} induction was not applied (Fig. 2j). Together, these results indicate that parental neuronal mitochondrial stress triggers an increase in mtDNA levels in the germline, which is subsequently inherited by descendants across generations through selection for strong UPR^{mt} induction.

Given that animals with elevated levels of mtDNA exhibited UPR^{mt}, we next examined the mitochondrial proteostasis stress by assessing the ratio between nDNA- and mtDNA-encoded proteins within the mitochondria¹⁵. Indeed, both TGW and TGQ animals displayed mitonuclear protein imbalances (Fig. 2k-m and Extended Data Fig. 4l-p). Furthermore, blue-native polyacrylamide gel

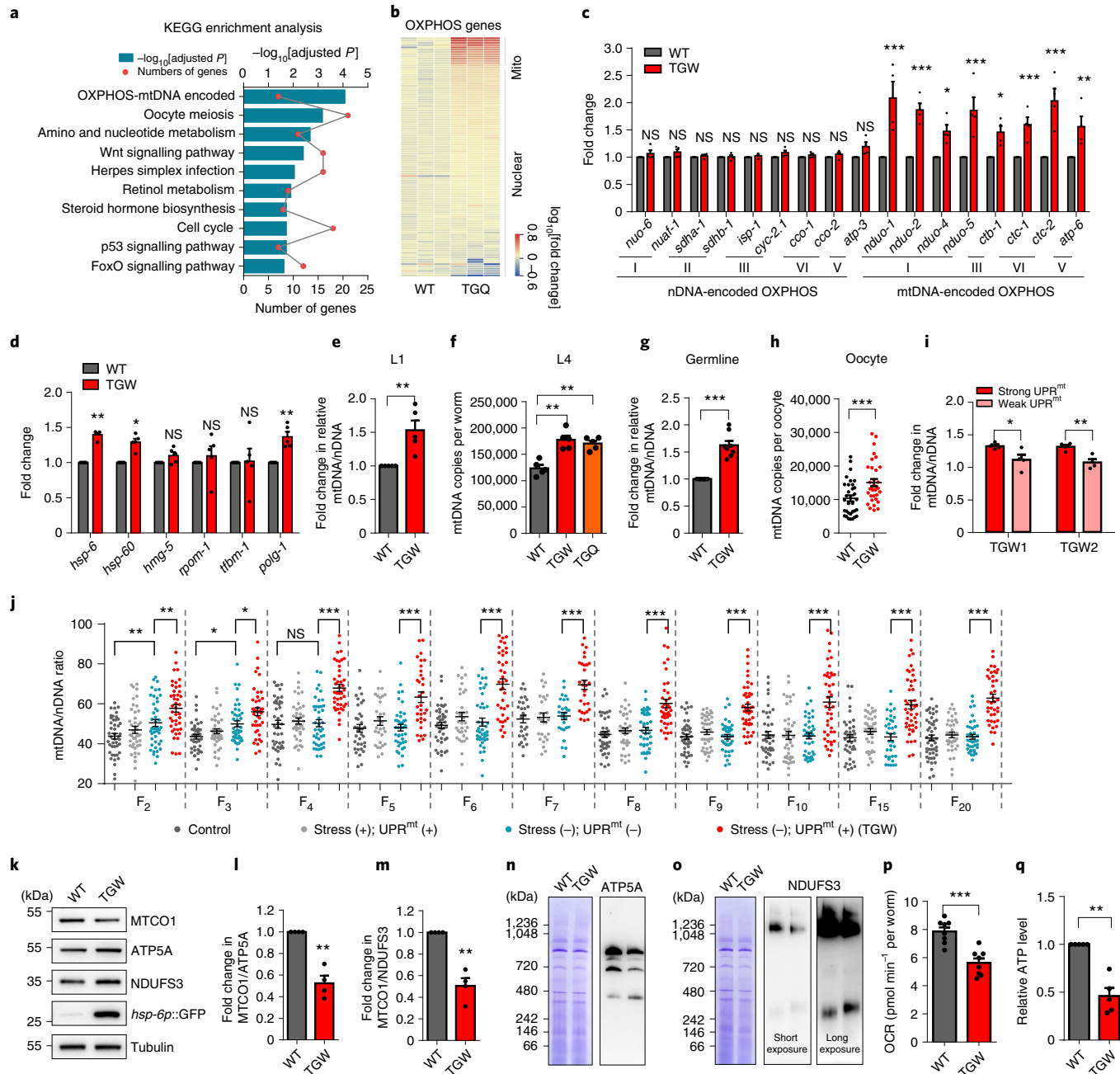


Fig. 2 | Descendants with transgenerational UPR^{mt} carry elevated levels of mtDNA. **a**, Gene Ontology–KEGG pathway analysis of differentially expressed genes in TGQ animals. **b**, Heat map of the \log_{10} -transformed fold change in the expression of OXPHOS genes in TGQ animals compared with the WT. **c**, qPCR with reverse transcription (RT-qPCR) analysis of the OXPHOS genes in TGW and WT animals. $n=4$ independent experiments. **d**, RT-qPCR analysis of mitochondrial genes in TGW and WT. $n=5$ independent experiments. **e**, The fold change in the mtDNA/nDNA ratios of TGW and WT animals at the L1 stage. $n=5$ independent experiments. **f**, mtDNA copy numbers per worm in TGW, TGQ and WT animals. $n=5$ independent experiments. **g**, The fold change in the mtDNA/nDNA ratios in the germline of TGW and WT animals. $n=8$ independent experiments. **h**, mtDNA copy numbers per oocyte (at position –1) of TGW and WT animals. $n=33$ oocytes. **i**, The fold change in the mtDNA/nDNA ratios of the strong and weak TGW animal populations. $n=4$ independent experiments. **j**, mtDNA/nDNA ratios of individual progeny generated from crosses between animals with neuronal Wnt and WT across generations as shown in Fig. 1a. $n \geq 30$ worms; exact n values are provided as source data. **k–m**, Representative immunoblots (**k**) and quantification (**l,m**) of mitochondrial OXPHOS proteins in TGW and WT animals, including mtDNA-encoded MTCO1, and nDNA-encoded ATP5A (**l**) and NDUFS3 (**m**). $n=4$ independent experiments. **n,o**, Western blot analysis of purified mitochondria from TGW and WT animals separated on a BN-PAGE gel and probed with antibodies against ATP5A (**n**) and NDUFS3 (**o**). **p,q**, The oxygen consumption rates (OCR) (**p**; $n=8$ independent experiments) and the ATP levels (**q**; $n=5$ independent experiments) of TGW and WT animals. Data are mean \pm s.e.m. *** $P < 0.001$, ** $P < 0.01$, * $P < 0.05$; NS, $P > 0.05$; P values were determined using the hypergeometric test and adjusted using the Benjamini–Hochberg method (**a**), two-way ANOVA (**c,d** and **i**), one-way ANOVA (**f**) and two-sided Student's *t*-tests (**e,g,h,j,l,m,p** and **q**). The exact P values are provided as source data. Source data are available online.

electrophoresis (BN-PAGE) revealed that more unassembled OXPHOS subunits accumulated within mitochondria in both TGW and TGQ animals than in WT animals (Fig. 2n,o and Extended Data Fig. 4q), accompanied by a reduced oxygen consumption rate and decreased ATP level (Fig. 2p,q and Extended Data Fig. 4r,s). Furthermore, a more punctate globular mitochondrial morphology was observed in the intestine, muscle cells and oocytes of TGW animals in contrast to the regular tubular appearance of mitochondria found in control animals (Extended Data Fig. 4t-v). Collectively, these results suggest that animals with increased levels of mtDNA exhibit mitonuclear protein imbalance and activate the UPR^{mt} in each generation.

The transmission of elevated mtDNA levels across generations.

To understand how the elevated levels of mtDNA were propagated across generations, we crossed TGW and TGQ hermaphrodites with males carrying either *atfs-1(gk3094)*, the transcription factor of the UPR^{mt}, or *lin-65(n3441)*, the epigenetic modifier of UPR^{mt}, and monitored two hallmarks of transgenerational effects—the mtDNA/nDNA ratio and the induction of the UPR^{mt} (refs. 18,22,36).

As compared with the TGW and TGQ animals, both TGW; *atfs-1*^{-/-} and TGQ; *atfs-1*^{-/-} mutants exhibited complete suppression of *hsp-6p::gfp* induction, which is consistent with the role of *atfs-1* in eliciting the UPR^{mt} (Fig. 3a-c and Extended Data Fig. 5a). However, the increase in relative mtDNA levels was not suppressed in TGW; *atfs-1*^{-/-} or TGQ; *atfs-1*^{-/-} animals (Fig. 3d and Extended Data Fig. 5b). Thus, TGW; *atfs-1*^{-/-} and TGQ; *atfs-1*^{-/-} animals still showed a mitonuclear protein imbalance (Fig. 3e-g and Extended Data Fig. 5c-e). When we restored ATFS-1 function by crossing the TGW; *atfs-1*^{-/-} animals with WT males, the suppression of *hsp-6p::gfp* was fully recovered in their descendants to the level observed in the TGW animals (Fig. 3a-d). Similarly, the *lin-65* mutants were also able to strongly suppress the UPR^{mt} but not the elevated mtDNA levels in TGW animals, and the suppression of *hsp-6p::gfp* was fully recovered after restoration of functional LIN-65 (Extended Data Fig. 5f-h).

To test whether the inheritance of increased mtDNA levels was established independently of the UPR^{mt} machinery, we generated TGW animals using parental animals completely lacking ATFS-1. The F₂ *atfs-1*-mutant animals (progeny of neuronal EGL-20; *atfs-1*^{-/-}_{herm} and *atfs-1*^{-/-}_{male}) still exhibited the increased relative mtDNA levels (Extended Data Fig. 5i). Collectively, these results indicate that the UPR^{mt} machinery is not required for either the establishment or transmission of the elevated mtDNA levels across generations, but it is essential for eliciting the UPR^{mt} in each generation.

The Wnt pathway is required for the transmission of elevated mtDNA levels across generations. Our previous study indicated that Wnt signalling is essential for the cell non-autonomous communication of the UPR^{mt} in *C. elegans*³². Given that the Wnt pathway was identified in KEGG analysis and that the mRNA levels of the Wnt ligand *egl-20* were significantly upregulated in both TGW and TGQ animals compared with WT animals (Fig. 2a and Extended Data Fig. 6a), we next investigated whether Wnt signalling is required for the observed transgenerational effects. TGW hermaphrodites were crossed with males carrying mutations in different Wnt signalling genes, namely the Wnt ligand (*egl-20*), the Wnt secretion receptor (*mig-14*) and the retromer component (*vps-35*). Loss of these Wnt signalling components completely suppressed the UPR^{mt}, as well as the increased relative mtDNA levels in both TGW and TGQ animals (Fig. 3h-k and Extended Data Fig. 6b,c). Furthermore, the mitochondrial proteostasis imbalance was restored in TGW; *egl-20*^{-/-} and TGQ; *egl-20*^{-/-} animals (Fig. 3l-n and Extended Data Fig. 6d-f). Thus, the UPR^{mt}-suppression phenotype remained even after the restoration of functional Wnt signalling in the descendants (Fig. 3h-k). Likewise, similar phenotypes

were observed in two other Wnt signalling mutants—*mig-14(ga62)* and *vps-35(ok1880)* (Extended Data Fig. 6g-l). Furthermore, none of the other Wnt ligands or Wnt receptors were found to be essential for the elevated mtDNA levels or the induction of UPR^{mt} in TGW animals (Extended Data Fig. 6m-o). Together, our results suggest that Wnt/EGL-20 pathway is required for the establishment and transmission of elevated mtDNA levels across generations.

To identify the tissues in which the Wnt pathway is required for the observed transgenerational phenotypes, we performed tissue-specific rescue experiments. Expression of *mig-14* in neurons completely restored the suppression of *hsp-6p::gfp* and elevated mtDNA levels in the TGW; *mig-14*^{-/-} animals (Fig. 3o-q), indicating that the restoration of functional Wnt signalling in the nervous system is sufficient to propagate the transgenerational signal to the offspring. Wnt ligands are known to not only act proximally to their sites of secretion, but also function from a distance to activate β-catenin (BAR-1), a downstream component of the Wnt pathway³⁷. RNAi against *bar-1* suppressed the induction of UPR^{mt} and the elevated mtDNA levels in descendants of TGW animals (Extended Data Fig. 6p-r). Knocking down *bar-1* specifically in the germline also strongly suppressed the elevated mtDNA levels of TGW animals, whereas knocking down *bar-1* in the intestine had no effect on the mtDNA levels (Fig. 3r,s and Extended Data Fig. 6q,r). Furthermore, *bar-1* RNAi resulted in decreased mitochondrial mass in the oocytes of WT worms (Fig. 3t,u). Collectively, these observations point to the Wnt-dependent transmission of the signal from neurons to the germline, which enables the transgenerational inheritance of elevated mtDNA levels and the induction of UPR^{mt}.

To determine whether the role of Wnt signalling in regulating mtDNA copy number is conserved in mammals, we activated Wnt signalling in the human cell line HEK293T using the GSK3 inhibitor CHIR-99021. There was a marked increase in relative mtDNA levels within hours of drug treatment in a dosage-dependent manner (Fig. 3v,w and Extended Data Fig. 6s-v). Furthermore, the increase in mtDNA levels was suppressed by siRNAs targeting the Myc transcription factor and β-catenin, two factors that are known to be involved in Wnt-mediated mtDNA biogenesis (Fig. 3x and Extended Data Fig. 6w,x).

Mitochondrial biogenesis and dynamic regulators mediate mtDNA levels. The level of mtDNA can be increased through mitochondrial biogenesis or decreased by elimination of damaged mitochondria through mitophagy³⁸. We found that the mtDNA levels of the WT controls and TGW animals were not significantly higher in the mitophagy mutant *pdr-1* or *pink-1* background (Fig. 4a,b). However, the mtDNA levels of parental animals with neuronal expression of Wnt/EGL-20 were substantially higher in the *pdr-1*- and *pink-1*-mutant backgrounds (Fig. 4a,b). Our results indicated that mitophagy might not have a predominant role in maintaining high mtDNA levels in animals lacking direct mitochondrial perturbations such as TGW animals.

Copies of mtDNA exist within mitochondria, which undergo dynamic fusion and fission to maintain mitochondrial homeostasis^{39,40}. Loss of the mitochondrial fusion regulator *fzo-1* completely suppressed the increase in relative mtDNA levels in TGW and TGQ animals, as *fzo-1* deficiency caused severe mtDNA depletion, whereas fission regulator *drp-1* deficiency did not cause significant differences in the relative mtDNA levels between WT and TGW and TGQ animals (Fig. 4c,d). However, the effects of *fzo-1* and *drp-1* on the UPR^{mt} in TGW and TGQ animals could not be evaluated as the loss of *fzo-1* or *drp-1* resulted in strong UPR^{mt} induction (Fig. 4e). Collectively, our results indicate that the maintenance of increased mtDNA levels is dependent on mitochondrial fusion, but not fission.

Animals lacking the mitochondrial DNA polymerase *polg-1* develop normally but do not produce viable progeny⁴¹. We found

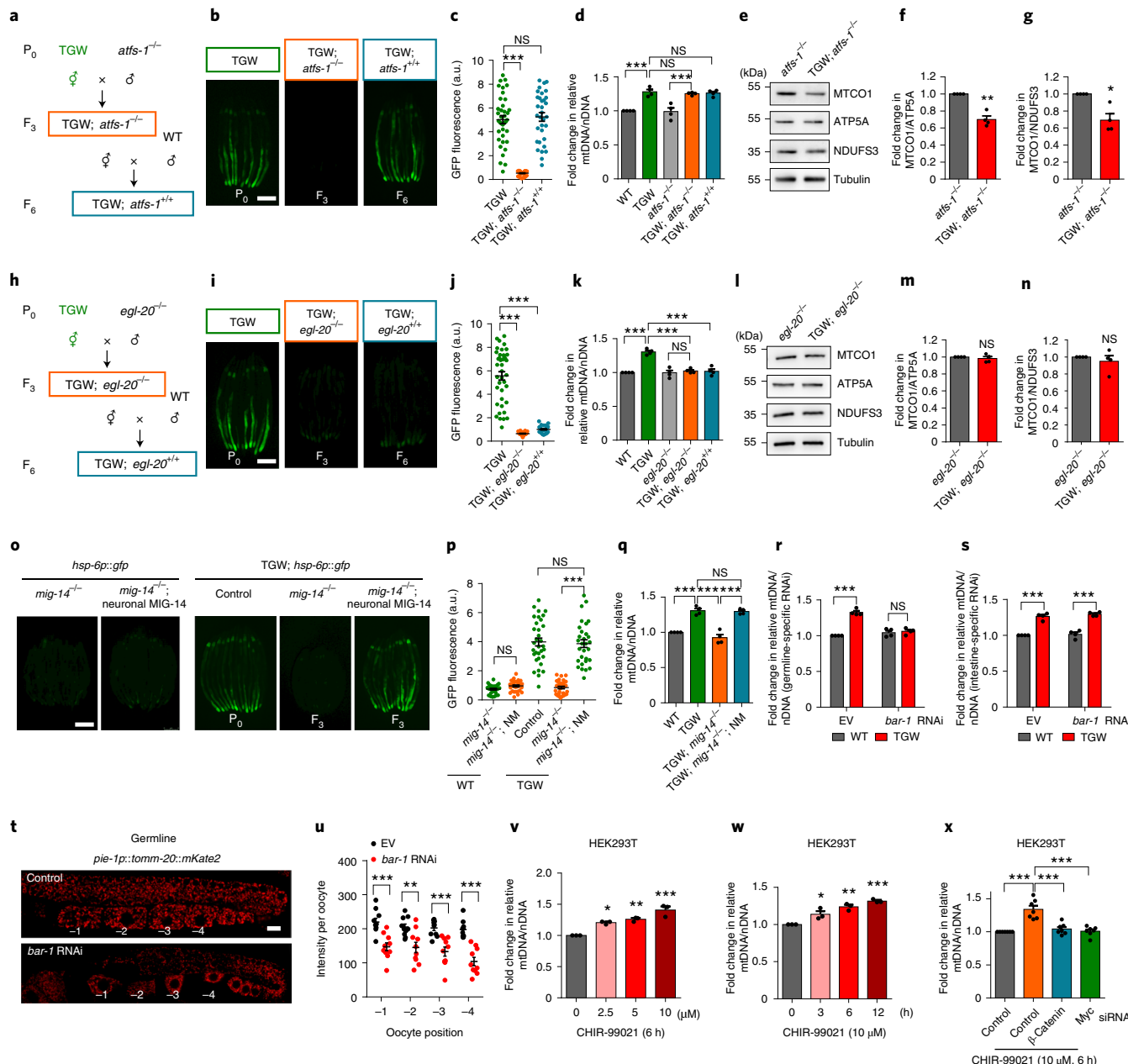


Fig. 3 | Wnt signalling is required for the transmission of elevated mtDNA levels across generations. **a-h**, The strategy used to induce mutants and restore gene function in TGW animals. **b,c**, Fluorescence visualization (**b**) and quantification (**c**) of the *hsp-6p:gfp* reporter in the indicated animals. $n=38$ (TGW), $n=34$ (TGW; *atfs-1^{-/-}*), $n=33$ (TGW; *atfs-1^{+/-}*) worms. Scale bar, 250 μ m. **d**, The fold change in mtDNA/nDNA ratios of animals shown in **b**. $n=4$ independent experiments. **e-g**, Representative immunoblots (**e**) and quantification of MTCO1/ATP5A (**f**) and MTCO1/NDUFS3 (**g**) in the indicated animals. $n=4$ independent experiments. **i-j**, Fluorescence visualization (**i**) and quantification (**j**) of the *hsp-6p:gfp* reporter in the indicated animals. $n=40$ (TGW), $n=31$ (TGW; *egl-20^{-/-}*) and $n=31$ (TGW; *egl-20^{+/-}*) worms. Scale bar, 250 μ m. **k**, The fold change in mtDNA/nDNA ratios of animals shown in **i**. $n=4$ independent experiments. **l-n**, Representative immunoblots (**l**) and quantification of MTCO1/ATP5A (**m**) and MTCO1/NDUFS3 (**n**) in the indicated animals. $n=4$ independent experiments. **o,p**, Fluorescence visualization (**o**) and quantification (**p**) of the *hsp-6p:gfp* reporter in TGW and WT worms in the *mig-14*-mutant background with or without neuronal MIG-14 rescue. $n \geq 30$ worms; the exact number of worms is provided as source data. Scale bar, 250 μ m. **q**, The fold change in the mtDNA/nDNA ratios of animals shown in **o**. $n=4$ independent experiments. **r,s**, The fold change in mtDNA/nDNA ratios of TGW and WT treated with EV or *bar-1* RNAi that is specifically functional in the germline (**r**) and intestine (**s**). $n=4$ independent experiments. **t,u**, The mitochondrial morphology (**t**) and mitochondrial content quantification (**u**) of oocytes in animals treated with EV and *bar-1* RNAi. Scale bar, 10 μ m. $n=10$ worms. **v-x**, The fold change in the mtDNA/nDNA ratios in HEK293T cells treated with CHIR-99021 at different concentrations (**v**) and for different times ($n=3$ independent experiments) (**w**) in combination with siRNA against β -catenin or Myc, normalized to the control ($n=7$ independent experiments) (**x**). Data are mean \pm s.e.m. P values were determined using two-way ANOVA (**r**, **s** and **u**), one-way ANOVA (**c**, **d**, **j**, **k**, **p**, **q**, **v**, **w** and **x**) and two-sided Student's t-tests (**f**, **g**, **m** and **n**); *** $P < 0.001$, ** $P < 0.01$, * $P < 0.05$; NS, $P > 0.05$. The exact P values are provided as source data. Source data are available online.

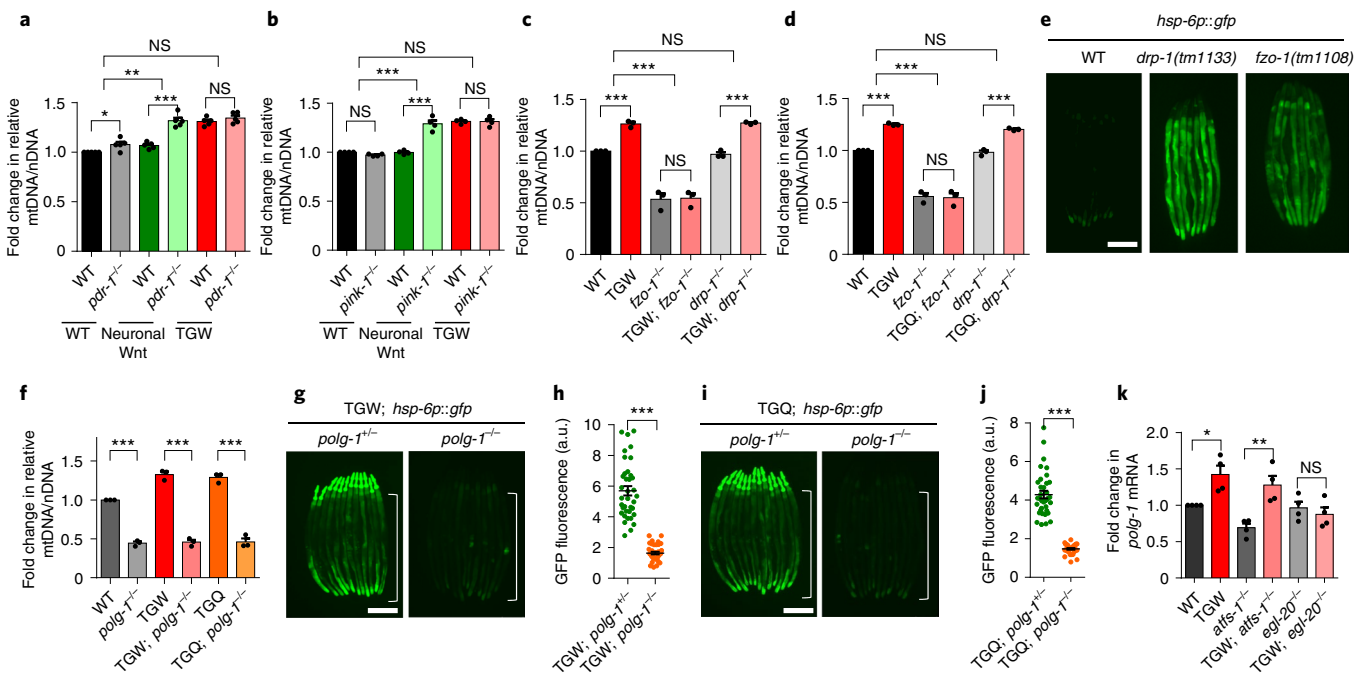


Fig. 4 | Mitochondrial fusion and mitochondrial DNA polymerase are required for the maintenance of elevated mtDNA levels. **a,b**, The fold change in the mtDNA/nDNA ratios of neuronal Wnt, TGQ and WT animals in the *pdr-1(gk448)* (**a**; $n=5$ independent experiments) and *pink-1(ok3538)* (**b**; $n=4$ independent experiments) backgrounds. **c,d**, The fold change in the mtDNA/nDNA ratios of TGW (**c**) and TGQ (**d**) and WT animals in the *fzo-1(tm1133)* and *drp-1(tm1108)* backgrounds. $n=3$ independent experiments. **e**, Fluorescence visualization of the *hsp-6p:gfp* reporter in the *drp-1* and *fzo-1*-mutant backgrounds. **f**, The fold change in the mtDNA/nDNA ratios of TGW, TGQ and WT animals in the *polg-1(tm2685)* background. *polg-1(tm2685)* homozygotes were sterile and a balancer *mlnT[dp-10(e128) mls14(myo-2::GFP)]* was introduced. $n=3$ independent experiments. **g,h**, Fluorescence visualization (**g**) and quantification (**h**) of the *hsp-6p:gfp* reporter in TGW; *polg-1^{+/-}* ($n=37$ worms), TGW; *polg-1^{-/-}* ($n=38$ worms) worms. **i,j**, Fluorescence visualization (**i**) and quantification (**j**) of the *hsp-6p:gfp* reporter in TGQ; *polg-1^{+/-}* ($n=32$ worms) and TGQ; *polg-1^{-/-}* ($n=34$ worms) worms. **k**, RT-qPCR analysis of *polg-1* transcripts of TGW and WT animals in the *egl-20^{-/-}* or *atfs-1^{-/-}* mutant background. $n=4$ independent experiments. Scale bars, 250 μ m. Data are mean \pm s.e.m. P values were determined using one-way ANOVA (**a-c**, **d**, **f** and **k**) and two-sided Student's t-tests (**h** and **j**); *** $P<0.001$, ** $P<0.01$, * $P<0.05$; NS, $P>0.05$. The exact P values are provided as source data. Source data are available online.

that the elevated mtDNA levels and the UPR^{mt} induction in TGW and TGQ animals were both strongly suppressed in homozygous *polg-1* mutants (Fig. 4f–j), suggesting that *polg-1* is indispensable for the elevated mtDNA levels. Moreover, the transcriptional upregulation of *polg-1* in TGW animals was dependent on *egl-20* but not *atfs-1* (Fig. 4k), consistent with the finding that the transgenerational elevated mtDNA level is dependent on Wnt signalling but not the UPR^{mt} pathway.

Wild C. elegans strains with higher levels of mtDNA. The diverse *C. elegans* wild strains exhibit phenotypic variation (for example, mtDNA levels) due to differences such as geographical origins and environmental factors. Among the wild strains we tested, ED3011 (ED) and KR314 (KR) had significantly higher ratios of mtDNA/nDNA compared with the reference strain N2 (refs. ^{42,43}; Fig. 5a). Notably, ED and KR also exhibited the induction of UPR^{mt} (Fig. 5b). Deep-sequencing analysis revealed that ED and KR strains exhibited significant genetic variation in both the nuclear and mitochondrial genomes compared with the reference strain N2. Nevertheless, these two strains shared numerous common genetic variations in their mtDNA that are not present in N2 or the Hawaiian strain CB4856 (Extended Data Fig. 7a,b and Supplementary Table 5)⁴².

To test whether inheritance of higher levels of mtDNA can induce the UPR^{mt}, we performed interstrain crosses and examined the levels of relative mtDNA as well as the UPR^{mt} in their progeny (F₁). We found that F₁ animals that inherited mitochondria from the ED and KR strains (N2; *hsp-6p:gfp_{male}* \times ED/KR_{herm}) showed stronger

induction of *hsp-6p:gfp* compared with the control F₁ animals (N2; *hsp-6p:gfp_{male}* \times N2_{herm}). By contrast, the F₁ animals generated from reciprocal crosses between ED/KR_{male} and N2; *hsp-6p:gfp_{herm}* that inherited mitochondria from N2 exhibited no difference in the induction of *hsp-6p:gfp* compared with control F₁ animals (N2_{male} \times N2; *hsp-6p:gfp_{herm}*) (Fig. 5c,d). Furthermore, the F₁ animals (ED/KR_{herm} \times N2_{male}) that inherited mitochondria exclusively from the ED and KR strains also retained higher levels of mtDNA compared with the corresponding F₁ animals generated from the reciprocal crosses (N2_{herm} \times ED/KR_{male}) with the same nuclear genomes but normal levels of mtDNA (Fig. 5e). Together, these results further demonstrated that transgenerational inheritance of higher levels of mtDNA can induce the UPR^{mt} in descendants.

The transgenerational effects of elevated mtDNA levels. To examine whether the transgenerational induction of the UPR^{mt} after inheritance of elevated mtDNA levels affects the physiology of worms, we assessed lifespan and stress resistance. Both TGW and TGQ animals lived significantly longer than their WT counterparts. This longevity was observed in multiple lines of TGW and TGQ animals across many generations, and was accompanied by a slightly delayed development and a reduced brood size (Fig. 6a–c and Extended Data Fig. 8a–d). As the activation of the UPR^{mt} response is transcriptionally associated with innate immune responses in *C. elegans*⁴⁴, we infected the TGW and TGQ animals with *Pseudomonas aeruginosa* (PA14), a pathogen that kills *C. elegans* within days of exposure⁴⁵. Remarkably, both TGW and TGQ

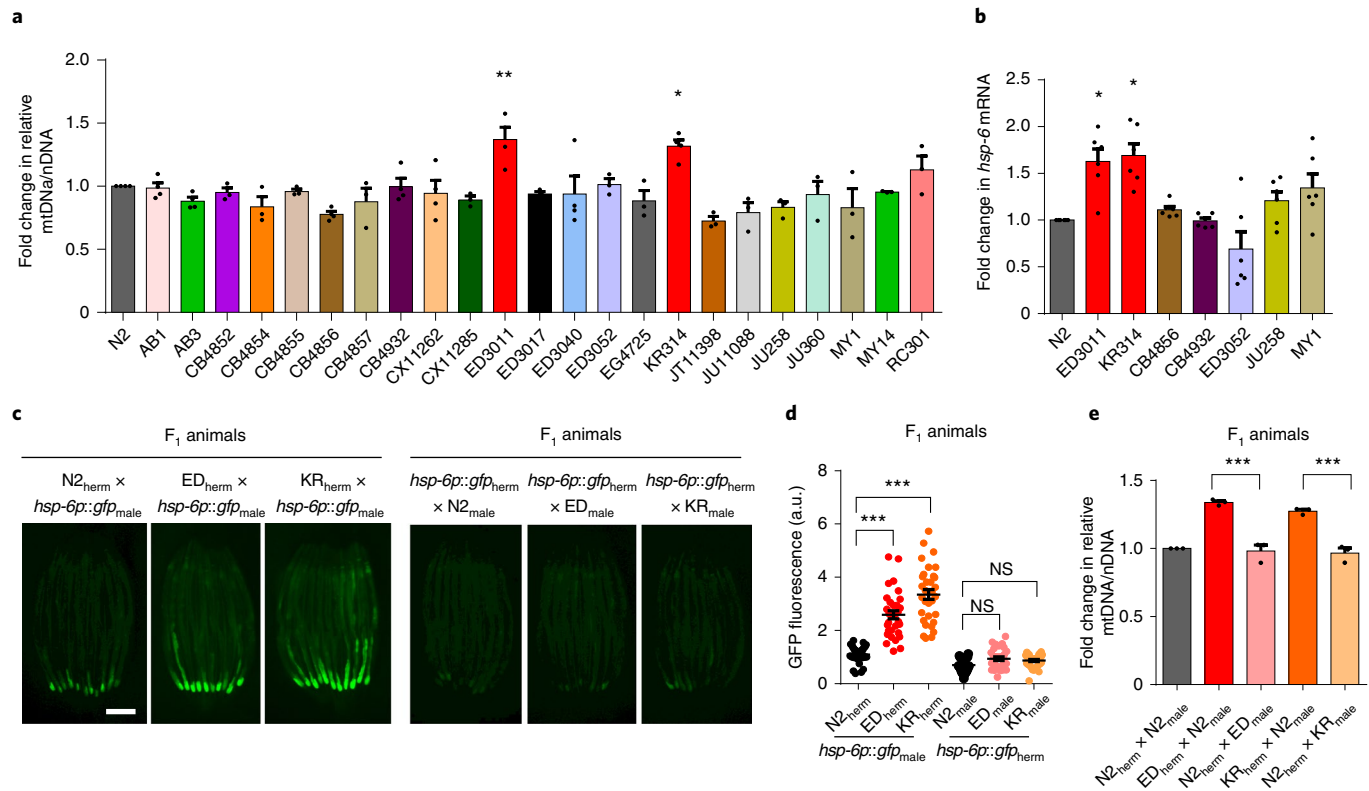


Fig. 5 | Higher levels of mtDNA inherited from wild *C. elegans* strains cause the induction of UPR^{mt} in descendants. **a**, The fold change in the mtDNA/nDNA ratios of different wild *C. elegans* strains. $n=3$ (CB4852, CB4854, CB4855, CB4857, CX11285, ED3011, ED3052, EG4725, JT11398, JU1088, JU258, JU360, MY1, MY14, RC301) and $n=4$ (N2, AB1, AB3, CB4856, CB4932, CX11262, ED3017, ED3040 and KR314) independent experiments. **b**, RT-qPCR analysis of UPR^{mt} target gene *hsp-6* in different wild *C. elegans* strains. $n=6$ independent experiments. **c,d**, Fluorescence visualization (**c**) and quantification (**d**) of the *hsp-6p::gfp* reporter in F₁ animals generated from reciprocal crosses between N2 (*hsp-6p::gfp*) and three different wild *C. elegans* strains (N2, ED3011 and KR314). $n=33$ (N2_{herm} × *hsp-6p::gfp*_{male}), $n=32$ (ED_{herm} × *hsp-6p::gfp*_{male}), $n=33$ (KR_{herm} × *hsp-6p::gfp*_{male}), $n=28$ (N2_{male} × *hsp-6p::gfp*_{herm}), $n=31$ (ED_{male} × *hsp-6p::gfp*_{herm}) and $n=35$ (KR_{male} × *hsp-6p::gfp*_{herm}) worms. **e**, The fold change in the mtDNA/nDNA ratios of F₁ animals generated from crosses between N2 and wild *C. elegans* strains ED3011/KR314 as described, normalized to N2 × N2. $n=3$ independent experiments. Data are mean ± s.e.m. *P* values were determined using one-way ANOVA (**a**, **b**, **d** and **e**); ****P* < 0.001, ***P* < 0.01, **P* < 0.05; NS, *P* > 0.05. The exact *P* values are provided as source data. Source data are available online.

animals survived significantly longer on PA14 lawns than the WT control animals (Fig. 6d and Extended Data Fig. 8e–h). Moreover, TGW and TGQ animals also exhibited resistance to heat stress and paraquat treatment (Fig. 6e,f and Extended Data Fig. 8i,j).

Both the ED and KR strains lived significantly longer than the N2 strain (Extended Data Fig. 8k). The F₁ animals (ED/KR_{herm} × N2_{male}) with higher ratios of mtDNA/nDNA exhibited significantly longer lifespans and increased resistance to paraquat treatment compared with their corresponding F₁ counterparts generated from the reciprocal cross (N2_{herm} × ED/KR_{male}) (Fig. 6g,h). Considering that the nuclear genetic background was almost identical between the F₁ animals generated from the reciprocal crosses, mtDNA levels and/or mitochondrial haplotype are probably the factors responsible for the phenotypic variation in the UPR^{mt}, stress resistance and lifespan.

Loss of *polg-1* and *fzo-1* suppressed the extended lifespan in both TGW and TGQ animals (Fig. 6i and Extended Data Fig. 8l,m). Similarly, loss of the Wnt ligand/*egl-20* and *atfs-1* also abolished the extended lifespan and increased resistance to heat and paraquat in both TGW and TGQ animals (Fig. 6j–q and Extended Data Fig. 8n,o). Thus, the elevated mtDNA levels as well as the subsequent induction of the UPR^{mt} are required for the longevity and stress resistance of offspring. Taken together, the transgenerational inheritance of elevated levels of mtDNA and the induction of the UPR^{mt} in the progeny enable animals to live longer and exhibit

increased resistance to stresses, at the cost of delayed development and reduced fecundity under favourable conditions.

Discussion

The impacts of parental experiences have been observed to extend over multiple generations in both human populations and experimental animal models^{4,5,13,46–48}. Given the ability of the nervous system to orchestrate the adaptive physiological responses across various tissues of the body, the question of whether neuronal stress signalling can induce heritable information in the germline, which can be passed onto progeny, is particularly intriguing. Studies in mice have shown that fear memory and olfactory experiences can be transmitted transgenerationally⁴⁹. However, at present there is scant evidence for the multigenerational effects of neuronal stresses^{50,51}. Our observation that neuronal mitochondrial stress can be sensed and responded to by the mitochondria in the germline to potentially promote the maternal inheritance of elevated mtDNA levels across multiple generations through Wnt signalling broadens the knowledge of transgenerational inheritance (Fig. 6r).

Isogenic *C. elegans* exhibited substantial interindividual variation in mtDNA copy number. However, the variability among TGW individuals did not seem to be significantly different from that among their unaffected siblings (*F* test, *P* > 0.05; details of the statistical analysis are available as source data), suggesting that selection on pre-existing mtDNA variation is probably not an explanation

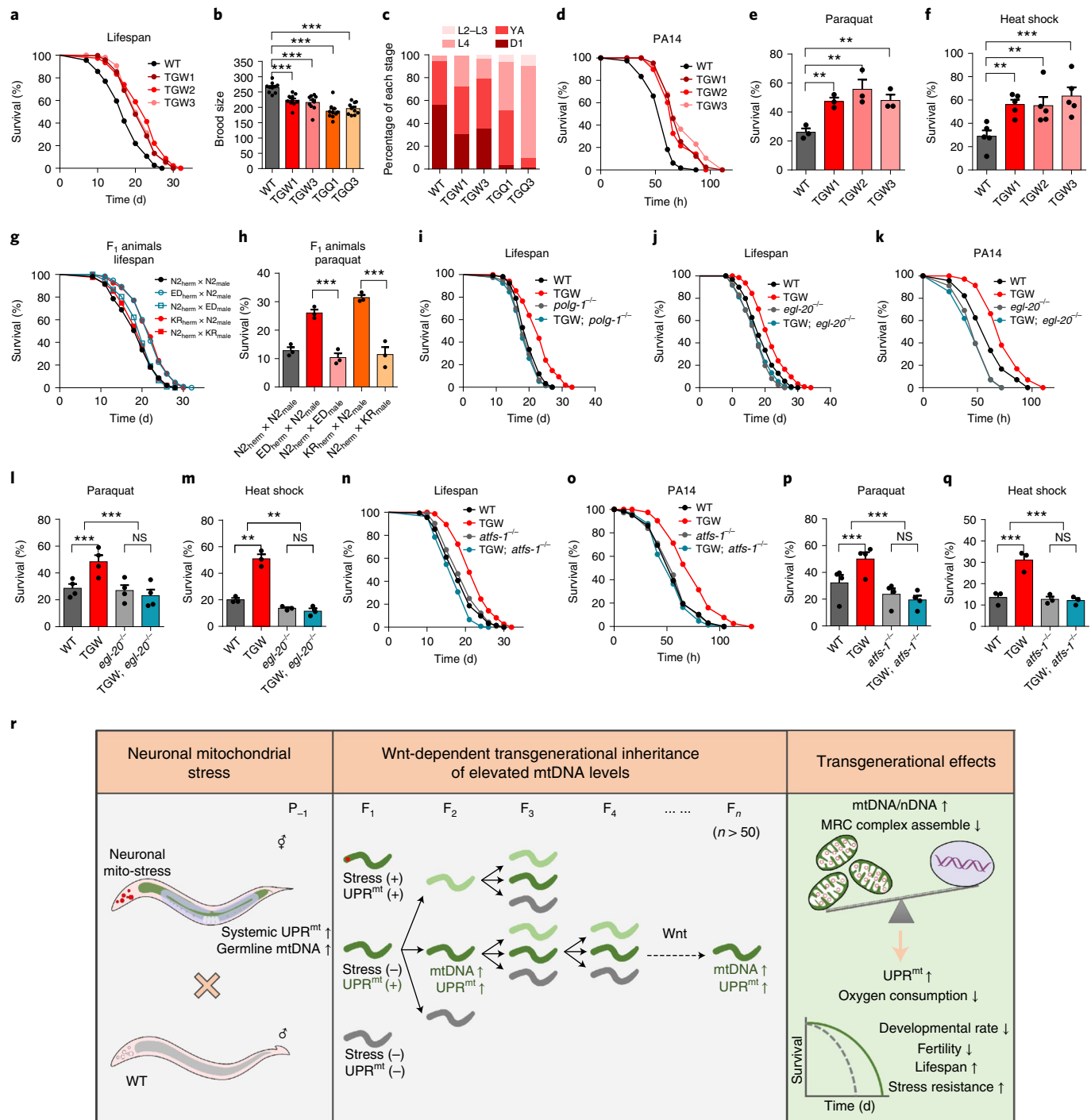


Fig. 6 | The transgenerational effects of elevated mtDNA levels. **a**, Lifespan analysis of TGW and WT animals. Three independent lines of TGW were examined with 5-fluoro-2'-deoxyuridine (FUDR) treatment. **b**, The brood size of TGW animals compared to WT animals. $n=10$ worms. **c**, The developmental rates of TGW animals compared to WT animals. **d**, PA14 slow-killing assay of TGW and WT animals. Three independent lines of TGW were examined with FUDR treatment. **e,f**, The survival rates of day-1 adult WT and TGW animals after paraquat (**e**, $n=3$ independent experiments) and heat shock (**f**; $n=5$ independent experiments) treatment. **g**, Lifespan analysis of F₁ animals generated from crosses between N2 and other wild C. elegans strains ED3011/KR314 as described. **h**, Lifespan rates of F₁ animals generated from crosses between N2 and wild strains ED3011/KR314 after paraquat treatment. $n=3$ independent experiments. **i**, Lifespan analysis of TGW animals in the *polg-1(tm2685)* background. **j,k**, Lifespan analysis (**j**) and PA14 slow-killing assay (**k**) of TGW animals in the *egl-20(rn585)* background. **l,m**, Survival rates of day-1 adult WT and TGW animals in the *egl-20(rn585)* background after paraquat (**l**; $n=4$ independent experiments) and heat shock (**m**; $n=3$ independent experiments) treatment. **n,o**, Lifespan analysis (**n**) and PA14 slow-killing assay (**o**) of TGW animals in the *atfs-1(gk3094)* background. **p,q**, Survival rates of day-1 adult WT and TGW animals in the *atfs-1(gk3094)* background after paraquat (**p**; $n=4$ independent experiments) and heat shock (**q**; $n=3$ independent experiments) treatment. **r**, Model for the transgenerational inheritance of increased mtDNA levels and the UPR^{mt}. Data are mean \pm s.e.m. P values were determined using one-way ANOVA (**b,e,f,h,l,m,p** and **q**); ***P < 0.001, **P < 0.01, *P < 0.05; NS, P > 0.05. The exact P values are provided as source data. Source data are available online.

for the observed transgenerational inheritance. The merit of the transgenerational inheritance of elevated mtDNA levels is fundamental because it might help the descendants to foresee and prepare for potential environmental challenges in the future; however, trade-offs are anticipated. The presence of such trade-offs implies a fitness cost of inheriting elevated mtDNA levels if stress conditions are not experienced in the future. Under these circumstances, these animals should be out-competed by animals without transgenerational inheritance, unless the animals with elevated levels of mtDNA gain a survival advantage under unfavourable conditions and increase their transmission frequency in a population.

It has been reported that mtDNA levels decrease with age, and studies have linked higher mtDNA levels to better physical and mental health status in aged populations^{52–55}. Consistent with the idea that increased mtDNA levels provide certain benefits, it has been proposed that duplication of the mitochondrial D-loop region is associated with increased longevity in bird species⁵⁶. The D-loop region is essential for the control of mtDNA copy number—it includes binding sites for both mtDNA replication enzymes and transcription factors⁵⁷. Bearing extra D-loop regions may result in increased mtDNA levels and/or in increased flexibility of cellular responses to stresses. Studies in conplastic mice with the same nuclear genome but different mtDNA variants indicated that mtDNA variations influence metabolic performances and aging, the phenomenon that is orchestrated by mitochondrial stress response pathways including the UPR^{mt} and ROS signalling⁵⁸.

The mitokine hypothesis was put forth to explain how mitochondrial stress in the nervous system could coordinate the systemic induction of the UPR^{mt} and the aging process. Here, we extended our understanding of mitokine signalling in the transmission of neuronal mitochondrial stress signals even across generations by increasing mtDNA levels in the germline of *C. elegans*. It will therefore be interesting to further investigate the role of Wnt signalling in the multigenerational plasticity related to mitochondrial physiology.

Online content

Any methods, additional references, Nature Research reporting summaries, source data, extended data, supplementary information, acknowledgements, peer review information; details of author contributions and competing interests; and statements of data and code availability are available at <https://doi.org/10.1038/s41556-021-00724-8>.

Received: 27 October 2020; Accepted: 29 June 2021;

Published online: 02 August 2021

References

- Rechavi, O. et al. Starvation-induced transgenerational inheritance of small RNAs in *C. elegans*. *Cell* **158**, 277–287 (2014).
- Chen, Q. et al. Sperm tsRNAs contribute to intergenerational inheritance of an acquired metabolic disorder. *Science* **351**, 397–400 (2016).
- Perez, M. F., Francesconi, M., Hidalgo-Carcedo, C. & Lehner, B. Maternal age generates phenotypic variation in *Caenorhabditis elegans*. *Nature* **552**, 106–109 (2017).
- Perez, M. F. & Lehner, B. Intergenerational and transgenerational epigenetic inheritance in animals. *Nat. Cell Biol.* **21**, 143–151 (2019).
- Skvortsova, K., Iovino, N. & Bogdanović, O. Functions and mechanisms of epigenetic inheritance in animals. *Nat. Rev. Mol. Cell Biol.* **19**, 774–790 (2018).
- Webster, A. K., Jordan, J. M., Hibshman, J. D., Chitrakar, R. & Baugh, R. L. Transgenerational effects of extended dauer diapause on starvation survival and gene expression plasticity in *Caenorhabditis elegans*. *Genetics* **210**, 263–274 (2018).
- Jobson, M. A. et al. Transgenerational effects of early life starvation on growth, reproduction, and stress resistance in *Caenorhabditis elegans*. *Genetics* **201**, 201–212 (2015).
- Baugh, L. R. & Day, T. Nongenetic inheritance and multigenerational plasticity in the nematode *C. elegans*. *eLife* **9**, e58498 (2020).
- Wallace, D. C. A mitochondrial paradigm of metabolic and degenerative diseases, aging, and cancer: a dawn for evolutionary medicine. *Ann. Rev. Genet.* **39**, 359–407 (2005).
- Shpilka, T. & Haynes, C. M. The mitochondrial UPR: mechanisms, physiological functions and implications in ageing. *Nat. Rev. Mol. Cell Biol.* **19**, 109–120 (2018).
- Ma, C. et al. N6-methyldeoxyadenine is a transgenerational epigenetic signal for mitochondrial stress adaptation. *Nat. Cell Biol.* **21**, 319–327 (2019).
- Hibshman, J. D., Hung, A. & Baugh, L. R. Maternal diet and insulin-like signaling control intergenerational plasticity of progeny size and starvation resistance. *PLoS Genet.* **12**, e1006396 (2016).
- Jordan, J. M. et al. Insulin/IGF signaling and vitellogenin provisioning mediate intergenerational adaptation to nutrient stress. *Curr. Biol.* **29**, 2380–2388 (2019).
- Okimoto, R., Macfarlane, J. L., Clary, D. O. & Wolstenholme, D. R. The mitochondrial genomes of two nematodes, *Caenorhabditis elegans* and *Ascaris suum*. *Genetics* **130**, 471–498 (1992).
- Houtkooper, R. H. et al. Mitonuclear protein imbalance as a conserved longevity mechanism. *Nature* **497**, 451–457 (2013).
- Martinus, R. D. et al. Selective induction of mitochondrial chaperones in response to loss of the mitochondrial genome. *Eur. J. Biochem.* **240**, 98–103 (1996).
- Yoneda, T. et al. Compartment-specific perturbation of protein handling activates genes encoding mitochondrial chaperones. *J. Cell Sci.* **117**, 4055–4066 (2004).
- Tian, Y. et al. Mitochondrial stress induces chromatin reorganization to promote longevity and UPR^{mt}. *Cell* **165**, 1197–1208 (2016).
- Merkwirth, C. et al. Two conserved histone demethylases regulate mitochondrial stress-induced longevity. *Cell* **165**, 1209–1223 (2016).
- Zhu, D. et al. NuRD mediates mitochondrial stress-induced longevity via chromatin remodeling in response to acetyl-CoA level. *Sci. Adv.* **6**, eabb2529 (2020).
- Benedetti, C., Haynes, C. M., Yang, Y., Harding, H. P. & Ron, D. Ubiquitin-like protein 5 positively regulates chaperone gene expression in the mitochondrial unfolded protein response. *Genetics* **174**, 229–239 (2006).
- Nargund, A. M., Pellegrino, M. W., Fiorese, C. J., Baker, B. M. & Haynes, C. M. Mitochondrial import efficiency of ATFS-1 regulates mitochondrial UPR activation. *Science* **337**, 587–590 (2012).
- Nargund, A. M., Fiorese, C. J., Pellegrino, M. W., Deng, P. & Haynes, C. M. Mitochondrial and nuclear accumulation of the transcription factor ATFS-1 promotes OXPHOS recovery during the UPR^{mt}. *Mol. Cell* **58**, 123–133 (2015).
- Durieux, J., Wolff, S. & Dillin, A. The cell-non-autonomous nature of electron transport chain-mediated longevity. *Cell* **144**, 79–91 (2011).
- Berendzen, K. M. et al. Neuroendocrine coordination of mitochondrial stress signaling and proteostasis. *Cell* **166**, 1553–1563 (2016).
- Lan, J. et al. Translational regulation of non-autonomous mitochondrial stress response promotes longevity. *Cell Rep.* **28**, 1050–1062 (2019).
- Higuchi-Sanabria, R., Frankino, P. A., Paul, J. W., Tronnes, S. U. & Dillin, A. A futile battle? Protein quality control and the stress of aging. *Dev. Cell* **44**, 139–163 (2018).
- Suomalainen, A. et al. FGF-21 as a biomarker for muscle-manifesting mitochondrial respiratory chain deficiencies: a diagnostic study. *Lancet Neurol.* **10**, 806–818 (2011).
- Owusu-Ansah, E., Song, W. & Perrimon, N. Muscle mitohormesis promotes longevity via systemic repression of insulin signaling. *Cell* **155**, 699–712 (2013).
- Kang, G. M. et al. Mitohormesis in hypothalamic POMC neurons mediates regular exercise-induced high-turnover metabolism. *Cell Metab.* **33**, 334–349 (2021).
- Shao, L. W., Niu, R. & Liu, Y. Neuropeptide signals cell non-autonomous mitochondrial unfolded protein response. *Cell Res.* **26**, 1182–1196 (2016).
- Zhang, Q. et al. The mitochondrial unfolded protein response is mediated cell-non-autonomously by retromer-dependent Wnt signaling. *Cell* **174**, 870–883 (2018).
- Taylor, R. C. & Dillin, A. XBP-1 is a cell-nonautonomous regulator of stress resistance and longevity. *Cell* **153**, 1435–1447 (2013).
- Lin, Y. F. et al. Maintenance and propagation of a deleterious mitochondrial genome by the mitochondrial unfolded protein response. *Nature* **533**, 416–419 (2016).
- Tsang, W. Y. & Lemire, B. D. Mitochondrial genome content is regulated during nematode development. *Biochem. Biophys. Res. Commun.* **291**, 8–16 (2002).
- Haynes, C. M., Yang, Y., Blais, S. P., Neubert, T. A. & Ron, D. The matrix peptide exporter HAF-1 signals a mitochondrial UPR by activating the transcription factor ZC376.7 in *C. elegans*. *Mol. Cell* **37**, 529–540 (2010).
- Korswagen, H. C. et al. The Axin-like protein PRY-1 is a negative regulator of a canonical Wnt pathway in *C. elegans*. *Genes Dev.* **16**, 1291–1302 (2002).

38. Narendra, D. P. et al. PINK1 is selectively stabilized on impaired mitochondria to activate Parkin. *PLoS Biol.* **8**, e1000298 (2010).
39. Silva Ramos, E. et al. Mitochondrial fusion is required for regulation of mitochondrial DNA replication. *PLoS Genet.* **15**, e1008085 (2019).
40. Jones, B. A. & Fangman, W. L. Mitochondrial DNA maintenance in yeast requires a protein containing a region related to the GTP-binding domain of dynamin. *Genes Dev.* **6**, 380–389 (1992).
41. Bratic, I. et al. Mitochondrial DNA level, but not active replicase, is essential for *Caenorhabditis elegans* development. *Nucleic Acids Res.* **37**, 1817–1828 (2009).
42. Maydan, J. S., Lorch, A., Edgley, M. L., Flibotte, S. & Moerman, D. G. Copy number variation in the genomes of twelve natural isolates of *Caenorhabditis elegans*. *BMC Genomics* **11**, 62 (2010).
43. Andersen, E. C. et al. Chromosome-scale selective sweeps shape *Caenorhabditis elegans* genomic diversity. *Nat. Genet.* **44**, 285–290 (2012).
44. Pellegrino, M. W. et al. Mitochondrial UPR-regulated innate immunity provides resistance to pathogen infection. *Nature* **516**, 414–417 (2014).
45. Tan, M. W., Mahajan-Miklos, S. & Ausubel, F. M. Killing of *Caenorhabditis elegans* by *Pseudomonas aeruginosa* used to model mammalian bacterial pathogenesis. *Proc. Natl Acad. Sci. USA* **96**, 715–720 (1999).
46. Mousseau, T. A. & Fox, C. W. The adaptive significance of maternal effects. *Trends Ecol. Evol.* **13**, 403–407 (1998).
47. Öst, A. et al. Paternal diet defines offspring chromatin state and intergenerational obesity. *Cell* **159**, 1352–1364 (2014).
48. Klosin, A., Casas, E., Hidalgo-Carcedo, C., Vavouris, T. & Lehner, B. Transgenerational transmission of environmental information in *C. elegans*. *Science* **356**, 320–323 (2017).
49. Dias, B. G. & Ressler, K. J. Parental olfactory experience influences behavior and neural structure in subsequent generations. *Nat. Neurosci.* **17**, 89–96 (2014).
50. Moore, R. S., Kaletsky, R. & Murphy, C. T. Piwi/PRG-1 argonaute and TGF- β mediate transgenerational learned pathogenic avoidance. *Cell* **177**, 1827–1841 (2019).
51. Posner, R. et al. Neuronal small RNAs control behavior transgenerationally. *Cell* **177**, 1814–1826 (2019).
52. Mengel-From, J. et al. Mitochondrial DNA copy number in peripheral blood cells declines with age and is associated with general health among elderly. *Hum. Genet.* **133**, 1149–1159 (2014).
53. Barazzoni, R., Short, K. R. & Nair, K. S. Effects of aging on mitochondrial DNA copy number and cytochrome c oxidase gene expression in rat skeletal muscle, liver, and heart. *J. Biol. Chem.* **275**, 3343–3347 (2000).
54. Ding, J. et al. Assessing mitochondrial DNA variation and copy number in lymphocytes of ~2,000 sardinians using tailored sequencing analysis tools. *PLoS Genet.* **11**, e1005306 (2015).
55. Wachsmuth, M., Hübner, A., Li, M., Madea, B. & Stoneking, M. Age-related and heteroplasmy-related variation in human mtDNA copy number. *PLoS Genet.* **12**, e1005939 (2016).
56. Skujina, I., McMahon, R., Lenis, V. P. E., Gkoutos, G. V. & Hegarty, M. Duplication of the mitochondrial control region is associated with increased longevity in birds. *Aging* **8**, 1781–1789 (2016).
57. Garesse, R. & Vallejo, C. G. Animal mitochondrial biogenesis and function: a regulatory cross-talk between two genomes. *Gene* **263**, 1–16 (2001).
58. Latorre-Pellicer, A. et al. Mitochondrial and nuclear DNA matching shapes metabolism and healthy ageing. *Nature* **535**, 561–565 (2016).

Publisher's note Springer Nature remains neutral with regard to jurisdictional claims in published maps and institutional affiliations.

© The Author(s), under exclusive licence to Springer Nature Limited 2021

Methods

C. elegans maintenance. *C. elegans* strains were maintained at 20 °C on standard nematode growth medium agar (NGM) plates seeded with *Escherichia coli* OP50 bacteria unless otherwise stated. A list of all strains used in this study is provided in Supplementary Table 2.

Cell culture and transfection. HEK293T cells were cultured in DMEM supplemented with 10% FBS and 1% penicillin–streptomycin at 37 °C under a CO₂ atmosphere. jetPRIME was used for siRNA transfection. All siRNAs were made by JTS scientific.

C. elegans mtDNA measurement by qPCR. mtDNA content was determined by qPCR for at least three biological replicates per strain using a previously described protocol with modifications³⁴. For each replicate, 30 early L4 (unless otherwise stated) worms were collected into 50 µl of worm lysis buffer containing 50 mM KCl, 10 mM Tris-HCl (pH 8.3), 2.5 mM MgCl₂, 0.45% NP-40, 0.45% Tween-20, 0.01% gelatin and fresh proteinase K (200 µg ml⁻¹). The worm lysate was then incubated at 65 °C for 100 min and 95 °C for 15 min. Subsequently, 3 µl of each sample was used as template in a qPCR assay using the Real-Time PCR Detection System (Bio-Rad) with the SYBR Green Real-time PCR Master Mix (TOYOBO QPK-201). *nduo-1* and *ges-1* were selected to quantify mtDNA and nDNA content, respectively. The mtDNA/nDNA ratio was then calculated using the comparative ΔΔC_t method. Fold changes of mtDNA/nDNA were normalized to the control in every single biological repeat. A list of the primers is provided in Supplementary Table 1.

For mtDNA content measurement at the single-worm level, an individual L4 worm was placed into 5 µl of worm lysis buffer, and mtDNA was isolated and quantified according to the protocol described above.

For germline-specific mtDNA content measurement, the heads of gravid D2 worms (~30) were cut off in 50 µl of M9 buffer on a poly-lysine coated slide, then two syringe needles were used to dissect the gonad of worms. Twenty dissected gonads were collected into 50 µl of worm lysis buffer using fine forceps (RWD, F11020-11), then mtDNA was quantified according to the protocol described above.

mtDNA measurement by ddPCR. Ten synchronized early L4 worms were collected into 50 µl of worm lysis buffer. The worm lysate was then incubated at 65 °C for 100 min and 95 °C for 15 min (protocol modified from the mtDNA measurement by qPCR protocol). Lysates were diluted 1:20 in water (nuclease-free), 4 µl of diluted lysate was used as template for a droplet digital PCR (ddPCR) reaction of the mtDNA measurement. For quantification of nDNA, the lysate was diluted 1:2. Primers were diluted to 1 µM in nuclease-free water, and 2 µl of each primer was combined with 4 µl of diluted lysate, 2 µl nuclease-free water and 10 µl QX200 ddPCR EvaGreen Supermix (Bio-Rad) to bring the reaction volume to 20 µl. Each ddPCR reaction was run on a QX200 Droplet Digital System (Bio-Rad) according to the standard manufacturer's protocol. A list of the primers is provided in Supplementary Table 1.

For oocyte-specific mtDNA content measurement, the heads of approximately 10 gravid D2 worms were cut off in 50 µl of M9 buffer on a poly-lysine coated slide. Each single oocyte (at position –1, which is located near the spermatheca) was transferred into 20 µl of worm lysis buffer using fine forceps (RWD, F11020-11). Lysates were diluted 1:4 in water (nuclease-free), then mtDNA was isolated and quantified according to the protocol described above, using 4 µl as template for a ddPCR reaction.

Drug treatment and mtDNA measurement for cells. HEK293T cells were seeded into six-well plates at a density of ~2.5 × 10⁵ cells per well. After 24 h, the medium was replaced and cells were treated with 10 µM of CHIR-99021. Then, 6 h later, cells were briefly washed in ice-cold PBS and collected in 600 µl cell lysis buffer containing 100 mM NaCl, 10 mM EDTA, 0.5% (w/v) SDS, 20 mM Tris-HCl (pH 7.4) and fresh proteinase K (200 µg ml⁻¹). The cell lysate was incubated at 55 °C for 12 h. The cell lysate was then boiled at 95 °C for 15 min and treated with RNase A. Next, DNA was extracted with isopropanol followed by a 70% ethanol wash. DNA (30 ng) was used as template in a qPCR assay using the Real-Time PCR Detection System (Bio-Rad) with the TOYOBO SYBR Green Real-time PCR Master Mix. mtDNA content was then normalized to nDNA content³⁵. A list of the primers is provided in Supplementary Table 1.

RNA extraction and RT-qPCR. Synchronized early L4 stage worms were collected with M9. TRIzol (500 µl; Invitrogen) was added to the tubes, which were then snap-frozen in liquid nitrogen. Samples were homogenized by repeatedly freezing in liquid nitrogen and thawing at 37 °C, and total mRNA was then extracted by chloroform treatment, followed by ethanol and isopropanol wash. DNA was wiped off using RQ1 RNase-Free DNase (Promega M6101). mRNA was extracted again with chloroform treatment, followed by an ethanol wash. Amplified cDNA was generated using the M-MLV Reverse Transcriptase kit (Thermo Fisher Scientific, 28025013). SYBR Green Real-time PCR experiments were performed using the Real-Time PCR Detection System (Bio-Rad) and the SYBR Green Real-time PCR Master Mix (TOYOBO QPK-201). Relative gene expression was normalized to *act-3* mRNA levels. Fold changes in gene expression were calculated using the

comparative ΔΔC_t method, and then normalized to the control for every single biological repeat. A list of the primers is provided in Supplementary Table 2. Each experiment was repeated three or more times with biological replicate samples.

RNAi feeding. For the RNAi feeding experiments, either the L4440 empty vector or the designated RNAi bacteria was used. Plates for RNAi analysis were prepared by supplementation of agar with 100 µg ml⁻¹ carbenicillin and 1 mM isopropyl-β-D-thiogalactoside after autoclaving. Worms were synchronized and grown from hatching on RNAi feeding plates unless otherwise stated. RNAi strains were from the Vidal library if present, or the Ahringer library if absent in the Vidal library.

Drug treatment. Worms were synchronized and eggs were placed onto NGM plates with seeded OP50, containing either 0.2 mM paraquat (dissolved in NGM) or 50 µl 0.01 M antimycin A (added to bacterial lawn on the top of the plates).

Paraquat killing assay. Synchronized day-1 adult worms of different strains were incubated in M9 containing 100 mM paraquat (Sigma-Aldrich, 36541) for 90 min at 20 °C, and recovered on a plate with seeded OP50 for 8 h before analysing the survival rate⁶⁰.

Heat shock resistance assay. Synchronized day-1 adult worms of different strains were incubated at 34 °C for 6 h, and recovered at 20 °C for 8 h before analysing the survival rate.

C. elegans slow-killing assay. Slow-killing experiments were performed as previously described⁴⁴ with minor modifications. *P. aeruginosa* was cultured in King's medium (tryptone (20 g l⁻¹), K₂HPO₄ (0.392 g l⁻¹), glycerol (15 mM l⁻¹), MgSO₄ (0.732 g l⁻¹), pH 7.2) for 12 h and then seeded onto slow-killing NGM agar plates (with 0.35% peptone). The plates were allowed to dry overnight at room temperature, then incubated at 37 °C for 24 h and allowed to equilibrate at room temperature. Synchronized day-1 worms were transferred from *E. coli* NGM plates to *P. aeruginosa* slow-killing plates and maintained at 25 °C. Animals were counted at the described times and were scored as dead if they failed to respond when touched. Each experiment was repeated at least three times and the log-rank (Mantel–Cox) statistical test was used to evaluate *P* values.

Lifespan assay. Lifespan assays were performed at 20 °C as previously described, the worms were scored for viability every second day, from day 1 of adulthood⁶¹. Lifespan assays were performed on *E. coli* OP50, unless otherwise indicated, and the animals were transferred to new plates with FUDR (200 µl of 10 mg ml⁻¹ 5-fluoro-2'-deoxyuridine was added to seeded plates) when they were at late L4 stage and again at day 5 of adulthood to avoid issues associated with early death through the 'bagging' phenotype. Prism 6 was used for statistical analysis, and the log-rank (Mantel–Cox) method was used to determine the level of significance.

Developmental rate assay. Worms were synchronized and 500 eggs of each strain were placed onto each NGM plates with seeded OP50. These worms grow at 20 °C for 70 h and the number of worms at each developmental stage was calculated.

Brood size assay. Ten synchronized L4 worms were placed onto NGM plates with seeded OP50 at 20 °C, and worms were transferred to fresh NGM plates every day. The total number of progenies was counted for each strain. The experiments were performed in at least three biological repeats and analysed using Student's *t*-tests.

Oxygen consumption. Oxygen consumption was measured using a Seahorse XFe96 analyzer at 20 °C as described previously¹⁵. Fifteen synchronized L4 worms of each strain were transferred into each well of a 96-well microplate containing 200 µl M9 buffer, 6 wells per strain. Basal respiration was measured for a total of 90 min, in 9 min intervals, which included a 3 min mix, a 3 min time delay and a 3 min measurement. The experiments were repeated at least three times for each strain. Student's *t*-tests were used to determine the level of statistical significance.

Imaging and analysis. Micrographs of whole-worm images were acquired using a Leica M165 FC dissecting microscope and LAS X software. Five to ten worms were anaesthetized using sodium azide (50 mM) before imaging. Exposure times were the same within each experiment. Fluorescent mitochondrial morphology images were taken using a Zeiss Imager M2 microscope. Unless otherwise noted, all animals used for images were day 2 adult hermaphrodites. All images are representative of more than three images. To quantify the intensity of GFP fluorescence, the entire region of the intestine was outlined and analysed using ImageJ software.

Western blot analysis. One hundred synchronized young adult worms were transferred into a tube containing 16 µl M9 buffer, which was then snap-frozen in liquid nitrogen and kept at –80 °C until all of the samples were ready for analyses. SDS loading buffer (5×) was added to each sample, mixed well and boiled for 15 min and resolved using Bio-Rad gels. Western blotting was performed using the following antibodies: anti-GFP (Santa Cruz Biotechnology, sc-9996, 1:1,000);

anti-tubulin (Sigma-Aldrich, T6074, 1:5,000); anti-ATP5A (Abcam, ab14748, 1:2,000), anti-NDUFS3 (Abcam, ab14711, 1:1,000); anti-MTCO1/COX1 (Abcam, ab14705, 1:500); and anti- β -catenin (BD, 610154, 1:1,000) antibodies; and anti-mouse secondary antibodies (EarthOx, E030110, 1:5,000). Protein bands or lanes were selected and the band intensity was calculated using ImageJ.

Mitochondrial preparation and BN-PAGE. BN-PAGE was performed essentially as described previously⁶³. In brief, synchronized early L4 stage worms were collected with M9. Worm lysates were obtained using a Teflon homogenizer (Wheaton, 358034) in MSME buffer (220 mM mannitol, 70 mM sucrose, 5 mM MOPS, 2 mM EDTA, 1 mM phenylmethylsulfonyl fluoride, pH 7.4) and centrifuged at 800g for 10 min. The supernatant was transferred into a new tube and centrifuged at 12,000g for 10 min. The supernatant was next discarded and the pellet was washed twice with MSME buffer. Mitochondrial proteins were solubilized using the NativePAGE Sample Prep Kit (Thermo Fisher Scientific, BN2008). Total protein (30 mg) was separated using a minigel system (Thermo Fisher Scientific, A25977) and commercial blue native gels (NativePAGE 3–12% Bis-Tris protein gels, 1.0 mm, 10 well; Thermo Fisher Scientific, BN1001BOX). The gels were stained with Coomassie Brilliant Blue R-250 solution according to the standard procedure. Western blotting of BN-PAGE gels was performed using polyvinylidene difluoride blotting membranes and the Mini Blot system (Thermo Fisher Scientific, B1000).

RNA-seq analysis. WT and TGQ animals were grown from hatching at 20 °C on NGM plates with seeded OP50 and collected by washing with M9 at the early L4 stage, followed by snap-freezing in liquid nitrogen. Total RNA was extracted from the worms using TRIzol Reagent according to the manufacturer's instructions (Invitrogen, 15596018) and genomic DNA was removed using RQ1 RNase-Free DNase (Promega, M6101). RNA quality was then determined using 2100 Bioanalyser (Agilent) and quantified using the ND-2000 (NanoDrop Technologies). Only high-quality RNA samples (optical density at 260 nm/280 nm ($OD_{260/280}$) = 1.8–2.2, $OD_{260/230}$ > 2.0, RNA integrity number (RIN) > 6.5, 28S:18S > 1.0, >2 μ g) were used to construct the sequencing library.

The RNA-seq transcriptome library was prepared according to the TruSeq™ RNA sample preparation Kit (Illumina) using 1 μ g of total RNA. In brief, first, mRNA was isolated according to the polyA selection method using oligo(dT) beads and then fragmented using fragmentation buffer. Second, double-stranded cDNA was synthesized using a SuperScript double-stranded cDNA synthesis kit (Invitrogen) using random hexamer primers (Illumina). Next, the synthesized cDNA was subjected to end-repair, phosphorylation and A-base addition according to Illumina's library construction protocol. Libraries were size-selected for cDNA target fragments of 200–300 bp on 2% Low Range Ultra Agarose and then PCR amplified using Phusion DNA polymerase (NEB) for 15 PCR cycles. After quantification by TBS380, the paired-end RNA-seq library was sequenced using the Illumina HiSeq X Ten (2 \times 150 bp read length) system.

The raw paired-end reads were trimmed and quality-controlled using SeqPrep (<https://github.com/jstjohn/SeqPrep>) and Sickle (<https://github.com/najoshi/sickle>) with the default parameters. Next, clean reads were separately aligned to the reference genome with orientation mode using TopHat (<http://tophat.ccb.umd.edu/>, v.2.0.0). The mapping criteria of bowtie was as follows: sequencing reads should be uniquely matched to the genome allowing for up to two mismatches, without insertions or deletions. The region of the genes was then expanded according to the depths of sites, and the operon was obtained. Moreover, the whole genome was split into multiple 15 kb windows that share 5 kb. New transcribed regions were defined as more than two consecutive windows without an overlapped region of the gene, where at least two reads mapped per window in the same orientation. To identify differentially expression genes (DEGs) between two different samples, the expression level of each transcript was calculated according to the fragments per kilobase of exon per million mapped reads method. RSEM (<http://deweylab.biostat.wisc.edu/rsem/>) was used to quantify gene abundances. Essentially, differential expression analysis was performed using DESeq2 (ref. ⁶³), DEGs with $|log_2\text{-transformed fold change}| > 1$ and adjusted $P < 0.05$ were considered to be significantly different expressed genes. Furthermore, functional-enrichment analysis of KEGG was performed to identify which DEGs were significantly enriched in pathways. Differentially expressed gene numbers of each pathway were shown. The P value of our KEGG pathway analysis was given by a hypergeometric test and the adjusted P value was calculated using the Benjamini–Hochberg method performed using the R function Padjust. Heat maps of all OXPHOS genes (cel00190) were generated from the KEGG pathway database (<http://www.genome.jp/kegg/>). Fold change was calculated by comparing the normalized count values of each TGQ animal to WT animal and then transformed to the \log_{10} scale. Heat maps were generated using TBtools⁶⁴. The complete list of enriched KEGG pathways and genes used to assemble heat maps is provided in Supplementary Table 4.

Deep sequencing. Animals were grown from hatching at 20 °C on NGM plates with seeded OP50 and collected by washing with M9 at the early L4 stage. Genomic DNA of each strain was extracted using the E.Z.N.A. Tissue DNA kit (Omega Bio-Tek) according to the Tissue DNA-Spin protocol. After the DNA

samples were delivered, a quality control test was performed on the specimens, and the qualifying DNA (>3 μ g; concentration, >30 ng μ l⁻¹; $OD_{260}/OD_{280} = 1.80$ –2.00) was used for further study.

For Illumina paired-end sequencing (PE150), at least 1 μ g genomic DNA was used for sequencing library construction for each sample. Paired-end libraries with insert sizes of ~450 bp were prepared according to Illumina's standard genomic DNA library preparation procedure. Purified genomic DNA was sheared into smaller fragments with a desired size by Covaris, and T4 DNA polymerase was applied to generate blunt ends. After adding an A base to the 3' end of the blunt phosphorylated DNA fragments, adapters were ligated to the ends of the DNA fragments. The desired fragments were purified using gel electrophoresis, and then selectively enriched and amplified by PCR. The index tag was introduced into the adapter at the PCR stage as appropriate followed by a library quality test. After quantification by TBS380, paired-end libraries were sequenced by Shanghai Biozero Biotechnology using the Illumina HiSeq PE system with 2 \times 150 bp read length.

The public data of reference genome of WBcel235 were obtained from the NCBI (BioProject: PRJNA13758). The raw paired-end reads were trimmed and quality controlled by Trimmomatic using the default parameters (<http://www.usadellab.org/cms/uploads/supplementary/Trimmomatic>). The high-quality sequencing reads were aligned to the WBcel235 reference genome sequence using BWA (<http://bio-bwa.sourceforge.net/>) with 'bwa mem' mode. After removing PCR-duplication reads using SAMtools (<http://samtools.sourceforge.net/>), the sequencing depth and coverage were calculated on the basis of the alignments using custom Perl scripts. The valid BAM file was used to detect SNPs and short indels using the GATK HaplotypeCaller function (<http://www.broadinstitute.org/gatk/>). Next, variant call format (VCF) files were generated by quality filtering (VariantFiltration with parameters: QD < 2.0 || FS > 60.0 || MQ 10.0). Furthermore, VCF files were filtered using VCFtools (v.0.1.11; parameters: --minQ 20 --minDP 4). When the gene annotation file of reference genome was provided, the annotation of detected variations was performed using ANNOVAR (<http://www.openbioinformatics.org/annovar/>), including SNPs (synonymous or non-synonymous mutations of SNPs) and indels. A complete list of genetic variations on mitochondrial genome identified in TGQ and TGW animals is provided in Supplementary Table 3. A complete list of genetic variations identified in wild *C. elegans* strains is provided in Supplementary Table 5.

Statistics and reproducibility. Experimental data were analysed using GraphPad Prism (v.6.01). For all graphs, the error bars indicate the mean \pm s.e.m. Differences were considered to be significant when $P < 0.05$. Statistical significance is indicated by asterisks; * $P < 0.05$; ** $P < 0.01$; *** $P < 0.001$. n represents the number of biological replicates unless otherwise indicated. No data were excluded from the analyses. To compare two normally distributed groups, two-tailed *t*-tests were used. For comparisons between multiple groups with one fixed factor, an ordinary one-way ANOVA or one-way repeated-measures ANOVA was used, followed by Dunnett's multiple-comparisons test or Tukey's multiple-comparisons test. For comparison between multiple groups with two fixed factors, an ordinary two-way ANOVA or two-way repeated-measures ANOVA was used with Sidak's multiple-comparisons test. The homogeneity of variances was tested using the *F* test. Lifespans and slow-killing assays were analysed using the Mantel–Cox log-rank test. All experiments were performed at least three times yielding similar results and comprised of biological replicates. All data points for all replicates for specific quantifications are provided in the source data.

Reporting Summary. Further information on research design is available in the Nature Research Reporting Summary linked to this article.

Data availability

The accession numbers for the raw sequencing files and the processed data reported in this paper are NCBI GEO: GSE157031, and NCBI BioProject: PRJNA607689 and PRJNA727630. Previously published DNA-sequencing data that were used here are available under accession code PRJNA13758. The KEGG pathway database used in this study is available online (<http://www.genome.jp/kegg/>). All other data supporting the findings of this study are available from the corresponding author on reasonable request. Source data are provided with this paper.

References

59. Quiros, P. M., Goyal, A., Jha, P. & Auwerx, J. Analysis of mtDNA/nDNA ratio in mice. *Curr. Protoc. Mouse Biol.* **7**, 47–54 (2017).
60. Rieckher, M., Markaki, M., Princz, A., Schumacher, B. & Tavernarakis, N. Maintenance of proteostasis by P body-mediated regulation of eIF4E availability during aging in *Caenorhabditis elegans*. *Cell Rep.* **25**, 199–211 (2018).
61. Dillin, A. et al. Rates of behavior and aging specified by mitochondrial function during development. *Science* **298**, 2398–2401 (2002).
62. van den Ecker, D. et al. Blue native electrophoresis to study mitochondrial complex I in *C. elegans*. *Anal. Biochem.* **407**, 287–289 (2010).

63. Love, M. I., Huber, W. & Anders, S. Moderated estimation of fold change and dispersion for RNA-seq data with DESeq2. *Genome Biol.* **15**, 550 (2014).
64. Chen, C. et al. TBtools: an integrative toolkit developed for interactive analyses of big biological data. *Mol. Plant* **13**, 1194–1202 (2020).

Acknowledgements

We thank the members of the Tian laboratory, D. Chen and X. Zhan for discussion and technical assistance; Y. Qi for the *polg-1* mutant strain; S. Zuryn for the germline mitochondrial marker strain; and S. Cai for the wild *C. elegans* strains. Several *C. elegans* strains used in this work were provided by CGC (supported by the NIH-Officer of Research Infrastructure Programs (P40 OD010440) and the Japanese National BioResource Project. This work was supported by the National Key R&D Program of China (2017YFA0506400, to Y.T.; and 2019YFA0508700, to W.Q.), the Strategic Priority Research Program of Chinese Academy of Sciences (XDB39000000, to Y.T.) and the National Natural Science Foundation of China (nos 31930023 and 31771333, to Y.T.; and no. 31922014, to W.Q.).

Author contributions

Y.T. and Q.Z. conceived the study and designed the experiments. Q.Z., Q.W., Z.W. and J.Z. performed the *C. elegans* crosses and western blotting. Q.Z., W.Z. and Q.W. performed the mtDNA measurement, qPCR experiments, lifespan experiments and

stress-resistance assay. Q.Z. performed BN-PAGE experiments, OCR measurement and data analysis. W.Z. performed the mtDNA measurement, qPCR experiments, western blotting in cell lines. X.L. performed the RNAi experiments and drug treatment. X.W. performed the ATP-level measurement. Y.G. and Y.L. performed plasmid and strain constructions. C.W. and W.Q. performed the RNA-seq analyses. Q.Z. prepared the original figures. Y.T. and Q.Z. wrote the manuscript.

Competing interests

The authors declare no competing interests.

Additional information

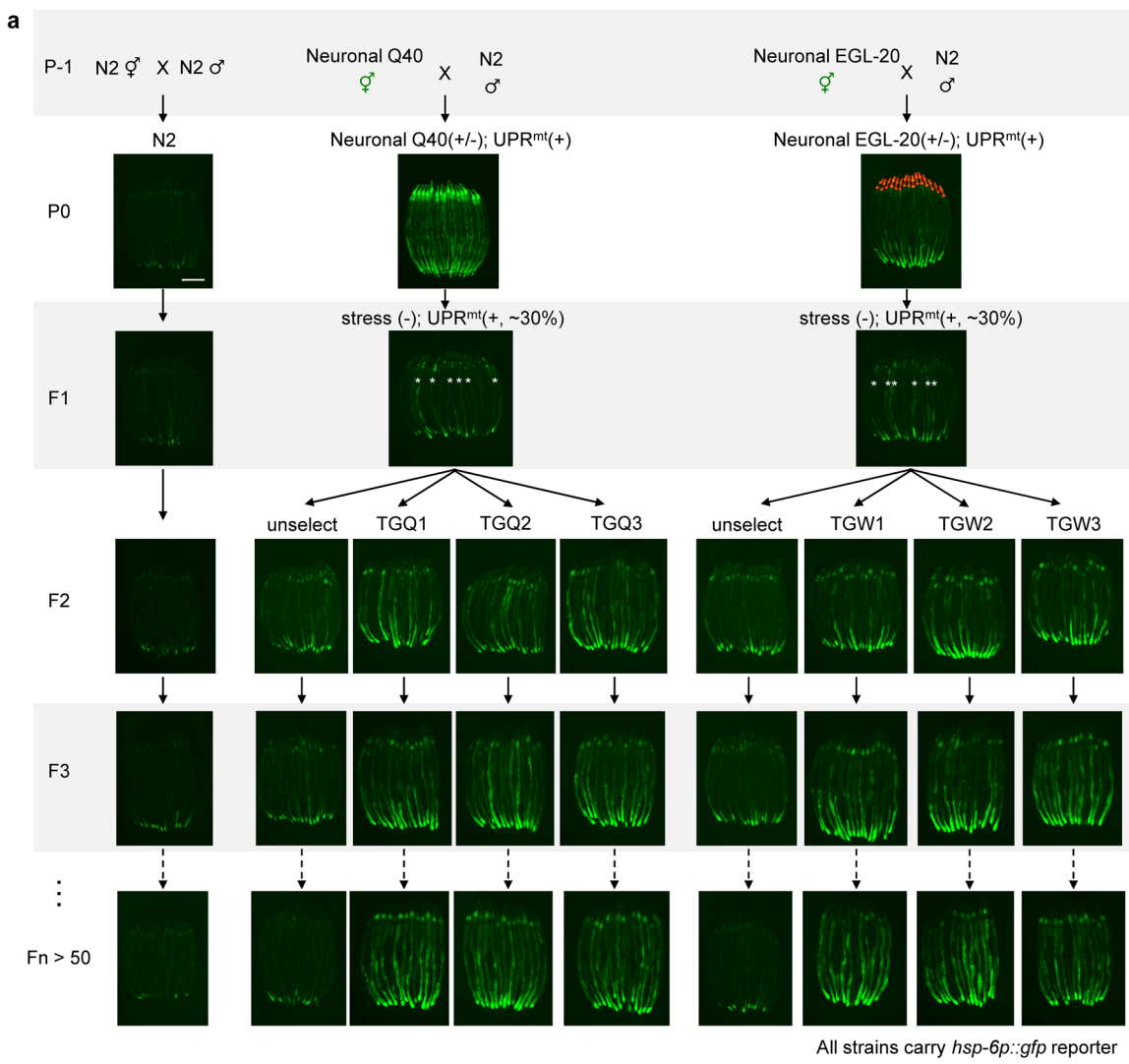
Extended data is available for this paper at <https://doi.org/10.1038/s41556-021-00724-8>.

Supplementary information The online version contains supplementary material available at <https://doi.org/10.1038/s41556-021-00724-8>.

Correspondence and requests for materials should be addressed to Y.T.

Peer review information *Nature Cell Biology* thanks Doris Germain, and the other, anonymous, reviewer(s) for their contribution to the peer review of this work. Peer review reports are available.

Reprints and permissions information is available at www.nature.com/reprints.



b

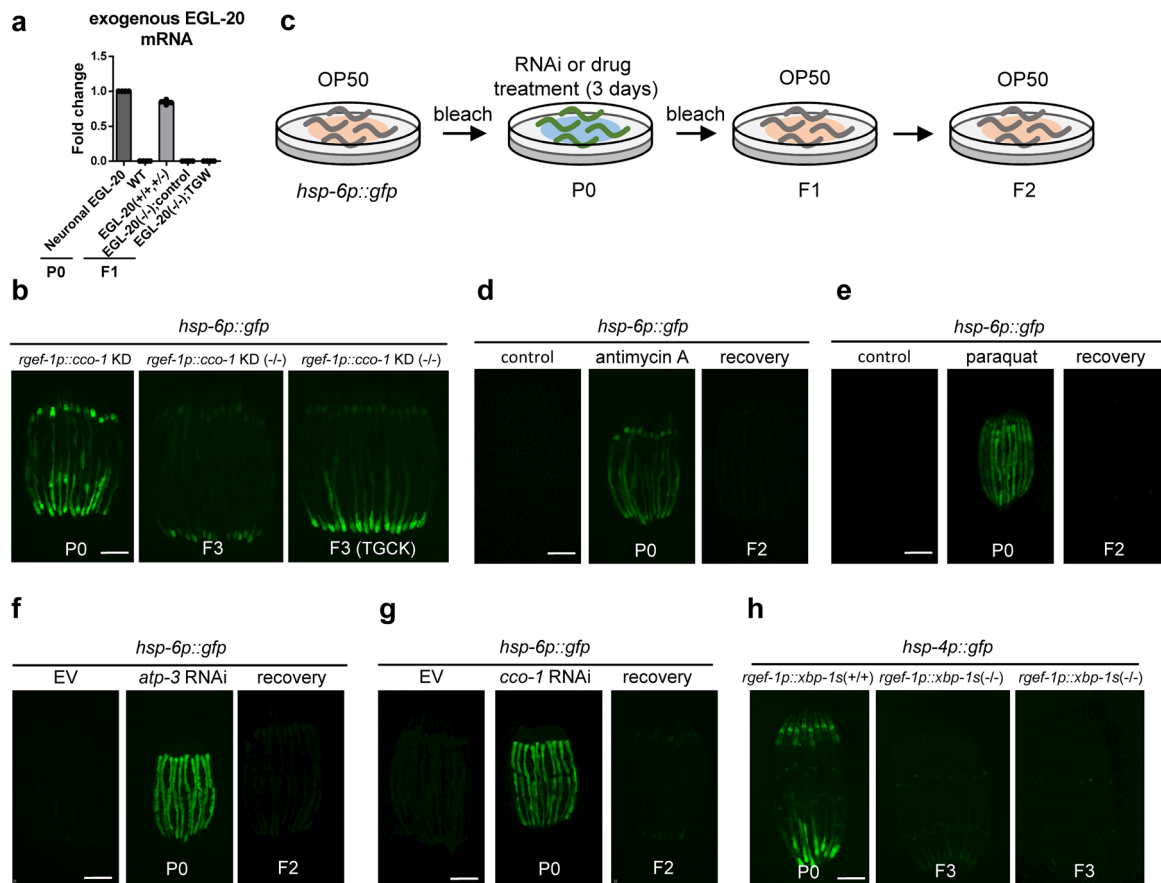
Generations	WT	<i>rgef-1p::Q40::YFP</i> (Neuronal Q40)				<i>rgef-1p::egl-20</i> (Neuronal Wnt)			
		unselect	TGQ1	TGQ2	TGQ3	unselect	TGW1	TGW2	TGW3
F1	5% (n=40)								31.5% (n=95)
F2	2.5% (n=40)	18% (n=50)	55.5% (n=36)	40% (n=40)	42.8% (n=42)	19.3% (n=52)	53.3% (n=45)	54.3% (n=35)	56.3% (n=32)
F3	5% (n=40)	10% (n=36)	84.4% (n=45)	69.8% (n=43)	70% (n=40)	20% (n=40)	78.9% (n=38)	85.7% (n=35)	87.8% (n=41)
F4	0% (n=40)	4.76% (n=42)	86.5% (n=37)	67.4% (n=43)	66.7% (n=45)	5% (n=40)	90.1% (n=44)	62.2% (n=37)	86.8% (n=38)
F5	0% (n=40)	0% (n=40)	85% (n=40)	77.7% (n=45)	70% (n=40)	0% (n=38)	82.9% (n=35)	85.7% (n=42)	90% (n=40)
F6	5% (n=40)	0% (n=35)	90.5% (n=42)	95% (n=40)	88.4% (n=43)	0% (n=41)	91.3% (n=46)	86.4% (n=44)	85% (n=40)
F7	0% (n=40)		78.9% (n=38)	89.7% (n=39)	90% (n=40)		85.4% (n=41)	85% (n=40)	88.9% (n=36)
F8	5% (n=40)		88.9% (n=45)	90.9% (n=44)	92.7% (n=38)		90% (n=40)	92.3% (n=39)	81.4% (n=43)
F9	0% (n=40)		87.5% (n=32)	91.4% (n=35)	78.0% (n=41)		81.4% (n=43)	75% (n=40)	87.0% (n=46)
F10	0% (n=40)		88.9% (n=45)	90% (n=40)	78.9% (n=38)		81.1% (n=37)	78.6% (n=42)	88.9% (n=45)
F11-50	0-5%		70-90%	70-90%	70-90%		70-90%	70-90%	70-90%

The penetrance of the UPR^{mt} induction in each generation.

Extended Data Fig. 1 | See next page for caption.

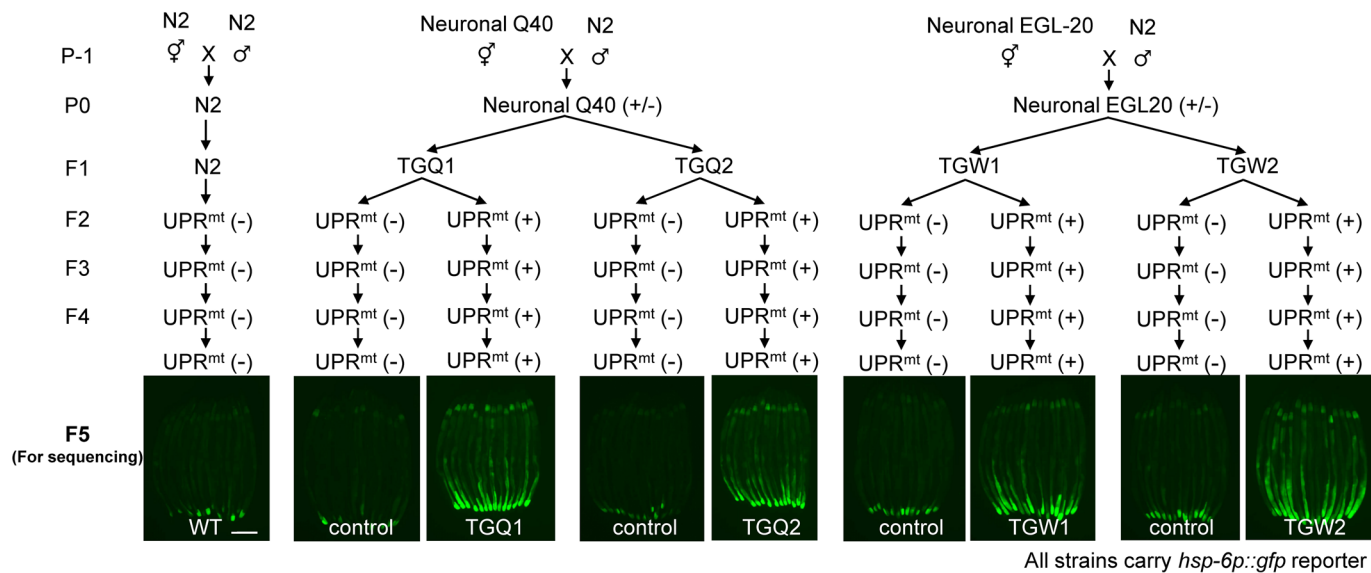
Extended Data Fig. 1 | Representative fluorescence visualization of the transgenerational induction of the UPR^{mt} across multiple generations.

a, Fluorescence visualization of the *hsp-6p::gfp* reporter in descendant animals generated from crosses between animals with neuronal mitochondrial stresses and wild-type animals. The schematic design of the experiment is presented in Fig. 1a. Worms with neuronal expression of Q40 or Wnt were crossed with WT males to generate the P0 animals with the expression of neuronal Q40 or Wnt. Then, P0 worms were allowed to produce F1 offspring through self-fertilization. 20%-30% of the F1 animals without expression of neuronal Q40 or Wnt still exhibited the strong induction of *hsp-6p::gfp* (indicated with white stars). We followed three independent lines with strong *hsp-6p::gfp* expression and one line that was not selected for the *hsp-6p::gfp* expression (randomly maintained) from each cross for over 50 generations. Worms with *hsp-6p::gfp* fluorescence over one-third of the intestine were considered to show the strong induction of the UPR^{mt}. Scale bar, 250 μ m. **b**, Percentage of worms showing the strong UPR^{mt} induction in each generation as shown in **a**.

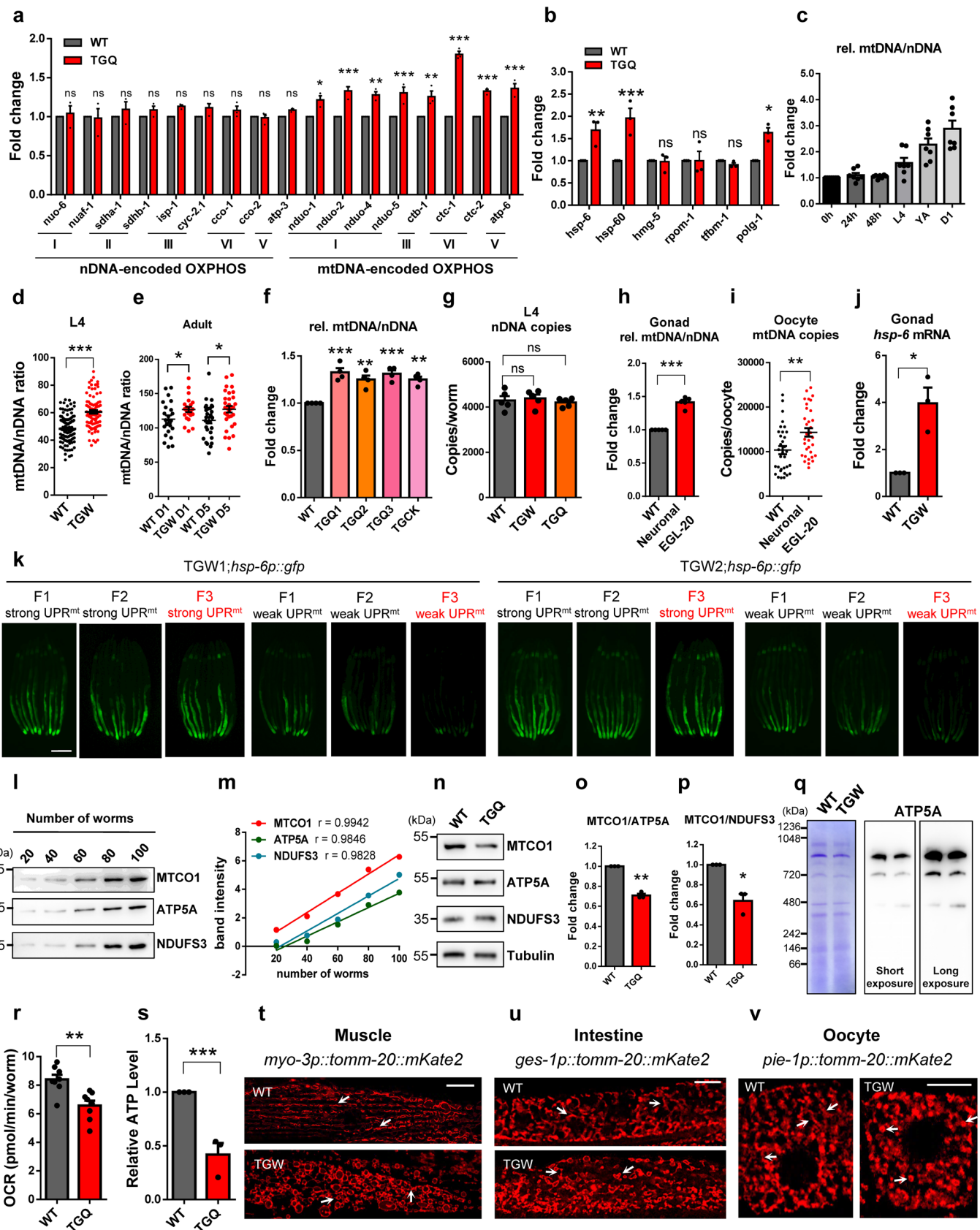


Extended Data Fig. 2 | Disrupting mitochondrial function by RNAi or drugs did not trigger the transgenerational induction of UPR^{mt} in their progeny.

a, qRT-PCR analysis of exogenous expression of neuronal *egl-20* in F1 animals with or without neuronal EGL-20 expression as described in Fig. 1d. n=4 independent experiments. **b**, Fluorescence visualization of the *hsp-6p::gfp* reporter in F1 animals with or without neuronal *cco-1* KD expression. Animals exhibiting the transgenerational induction of UPR^{mt} generated from animals with neuronal *cco-1* KD were referred to as 'TGCK'. Data shown represent five independent experiments with similar results. **c**, The schematic diagram of the strategy used to induce the UPR^{mt} in parental animals using RNAi or drug treatments and subsequently bleached these animals and transferred the progeny to the untreated plates. **d-g**, Fluorescence visualization of the *hsp-6p::gfp* reporter animals treated with different drugs and RNAi to perturb mitochondrial function, and their progeny recovered on OP50 plates as described. Data shown represent five independent experiments with similar results. **h**, Fluorescence visualization of the *hsp-4p::gfp* reporter in F1 animals with or without neuronal spliced *xbp-1s*. No transgenerational induction of UPR^{mt} was observed. Data shown represent five independent experiments with similar results. Scale bars, 250 µm. Data are the mean ± s.e.m.. Statistics source data are provided.

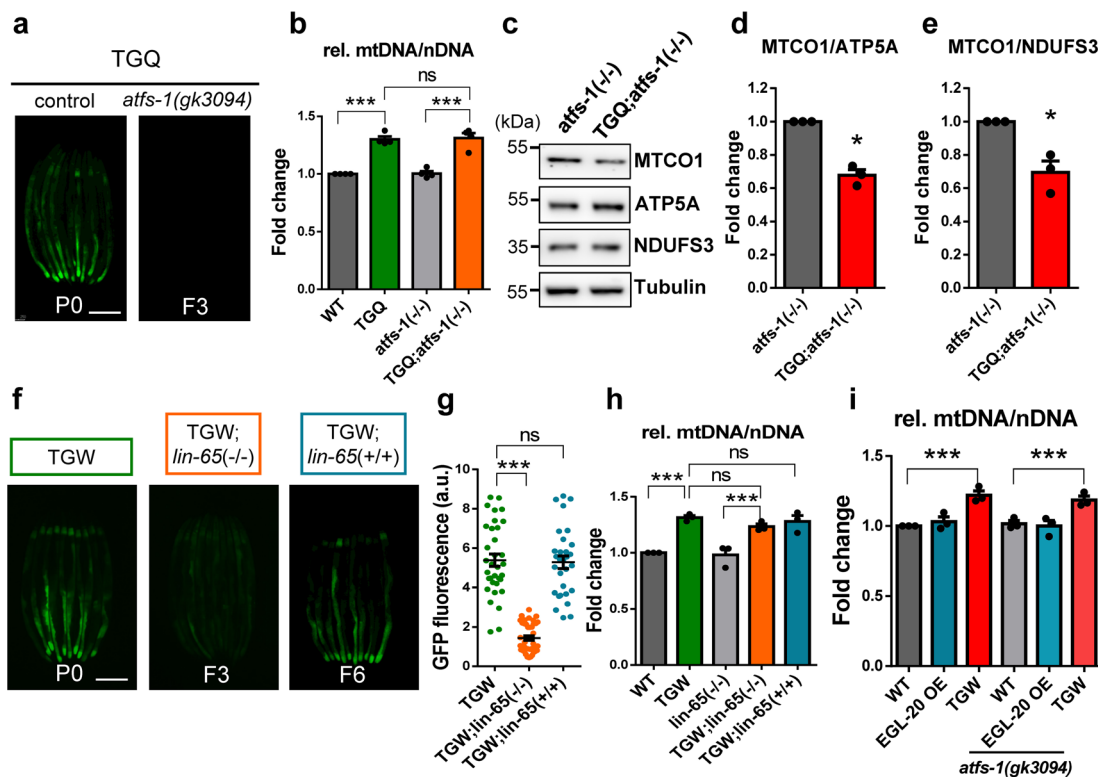


Extended Data Fig. 3 | A schematic design of experiment to generate animals with the transgenerational induction of the UPR^{mt} for mtDNA sequencing. Worms used for the mtDNA sequencing are P0 animals with expression of neuronal Q40 or neuronal Wnt, and their F5 progeny with or without UPR^{mt} induction. Data shown represent five independent experiments with similar results. Scale bar, 250 μm.

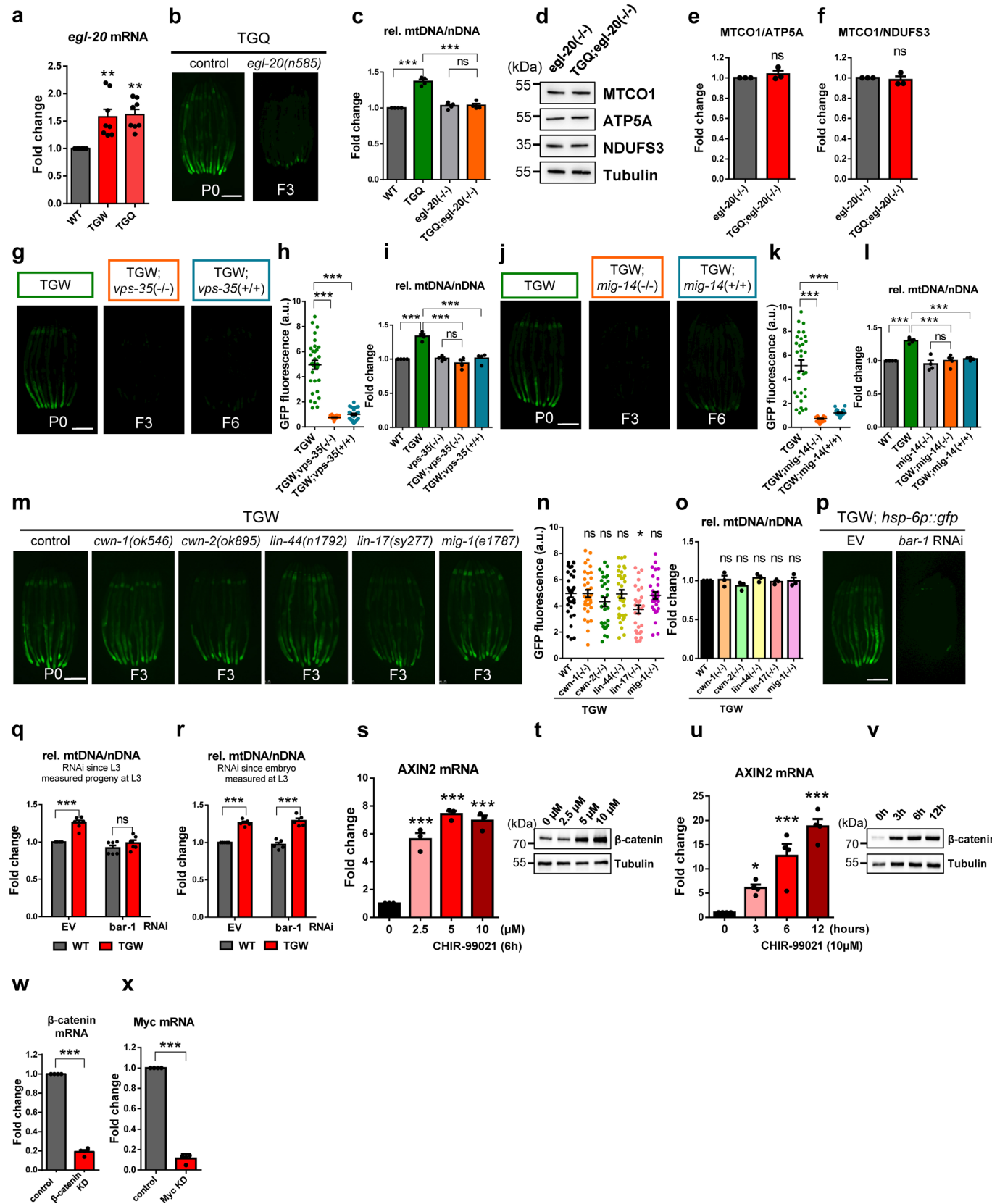


Extended Data Fig. 4 | See next page for caption.

Extended Data Fig. 4 | Animals with elevated levels of mtDNA causes mitochondrial proteostasis stress. **a**, qRT-PCR analysis of nDNA-encoded and mtDNA-encoded OXPHOS genes in TGQ and WT animals. $n=3$ independent experiments. **b**, qRT-PCR analysis of UPR^{mt} target genes and *polg-1*, *hmg-5*, *rpom-1*, *tfbm-1* in TGQ and WT animals. $n=3$ independent experiments. **c**, Relative mtDNA levels of WT worms at different developmental stages. $n=7$ independent experiments. **d, e**, mtDNA/nDNA ratios of TGW and WT animals. WT $n=102$ worms, TGW $n=89$ worms, WT D1 $n=22$ worms, TGW D1 $n=22$ worms, WT D5 $n=30$ worms, TGW D5 $n=31$ worms. **f**, Fold change in mtDNA/nDNA ratios of animals exhibited transgenerational UPR^{mt} generated from animals with neuronal Q40 expression, or neuronal *cco-1* KD. $n=4$ independent experiments. **g**, Actual nDNA copies per worm of TGW, TGQ and WT animals. $n=5$ independent experiments. Related to Fig. 2f. **h**, Fold change in germline mtDNA/nDNA ratios of animals expressing neuronal EGL-20 compared to WT. $n=5$ independent experiments. **i**, Actual mtDNA copies per oocyte (position at ‘-1’, the one near to the spermatheca) of animals expressing neuronal EGL-20 compared to WT. $n=33$ oocytes. **j**, qRT-PCR analysis of *hsp-6* transcripts in the germline of TGW and WT animals. $n=3$ independent experiments. **k**, Fluorescence visualization of the *hsp-6p::gfp* reporter in two groups of TGW animals according to their *hsp-6p::gfp* fluorescent intensities. Data shown represent three independent experiments with similar results. Scale bar, 250 μ m. **l, m**, Representative immunoblots (**l**) and quantifications (**m**) of antibody sensitivity by western blot analyses of WT worms. **n-p**, Representative immunoblots (**n**) and quantifications (**o, p**) of mitochondrial OXPHOS proteins in TGQ and WT animals. $n=3$ independent experiments. **q**, Western blot of purified mitochondria from TGQ and WT worms separated by Blue-native page gel using antibody against ATP5A (complex V). **r**, The oxygen consumption rates (**r**, $n=8$ independent experiments) and the relative ATP levels (**s**, $n=3$ independent experiments) of TGQ and WT animals. **t-v**, The mitochondria morphology in muscle (**t**), intestine (**u**), and oocytes (**v**) in TGW and WT worms. Scale bars, 10 μ m. Data shown represent three independent experiments with similar results. Data are the mean \pm s.e.m., *** $P<0.001$, ** $P<0.01$, * $P<0.05$, ns denotes $P>0.05$, P values were determined using two-way ANOVA (**a, b**), one-way ANOVA (**f, g**) and two-sided Student’s *t*-test (**d, e, h, i, j, o, p, r, s**). The exact P values are provided in Source Data Extended Data Fig. 4. Statistics source data and unprocessed western blots are provided.

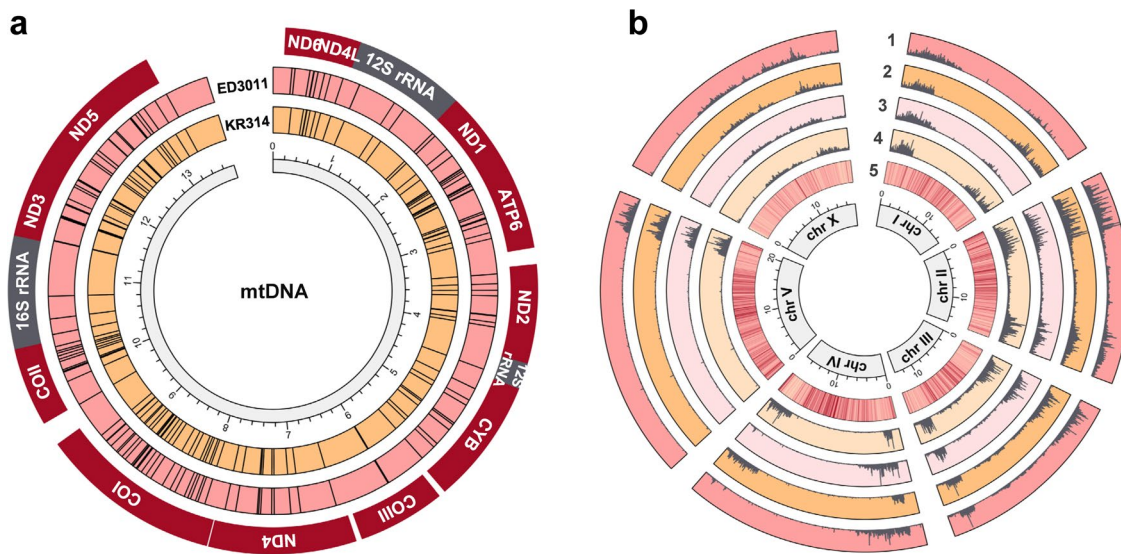


Extended Data Fig. 5 | UPR^{mt} machinery is not required for the transmission of increased mtDNA levels across generations. **a, b**, Fluorescence visualization of the *hsp-6p::gfp* reporter (**a**) and fold change in relative mtDNA levels (**b**) in TGQ, TGQ; *atfs-1(-/-)* animals. n = 4 independent experiments. **c–e**, Representative immunoblots (**c**) and quantifications (**d, e**) of mitochondrial OXPHOS proteins in *atfs-1* and TGQ; *atfs-1* animals. n = 3 independent experiments. **f, g**, Fluorescence visualization (**f**) and quantifications (**g**) of the *hsp-6p::gfp* reporter in TGW, TGW; *lin-65(-/-)* and TGW; *lin-65(+/+)* animals. TGW n = 34 worms, TGW; *lin-65(-/-)* n = 41 worms, TGW; *lin-65(+/+)* n = 30 worms. **h**, Fold change in mtDNA/nDNA ratios of animals shown in (**f**). n = 3 independent experiments. **i**, Relative mtDNA levels in F1 animals generated from the cross between neuronal EGL-20; *atfs-1(gk3094)* hermaphrodites and *atfs-1(gk3094)* males. The cross strategy was described in Fig. 1a. n = 3 independent experiments. Scale bars, 250 μ m. Data are the mean \pm s.e.m. ***P < 0.001, **P < 0.01, *P < 0.05, ns denotes P > 0.05, P values were determined using one-way ANOVA (**b, g, h, i**) and two-sided Student's t-test (**d, e**). The exact P values are provided in Source Data Extended Data Fig. 5. Statistics source data and unprocessed western blots are provided.

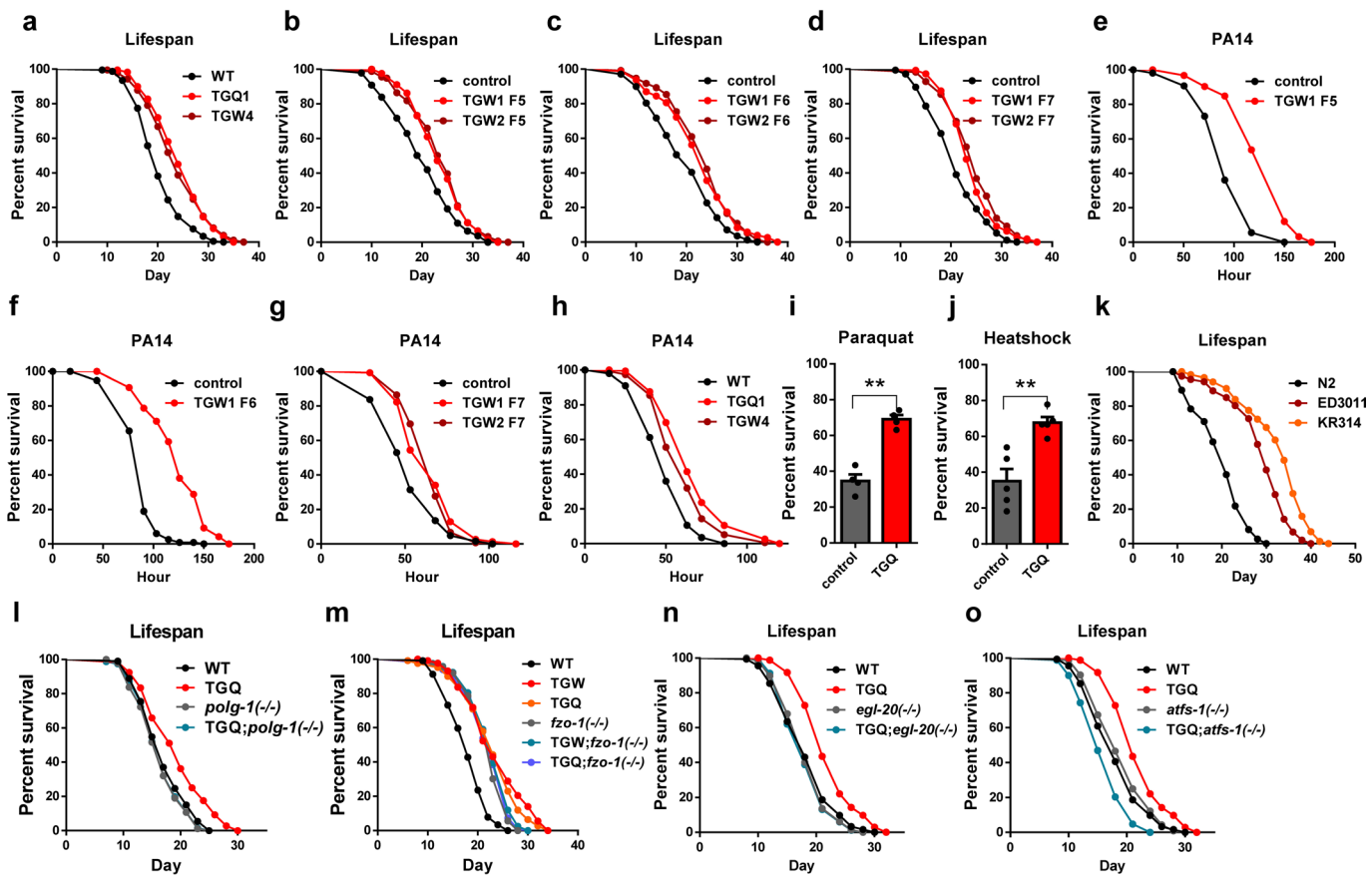


Extended Data Fig. 6 | See next page for caption.

Extended Data Fig. 6 | Wnt signaling is involved in the transmission of increased mtDNA levels across generations and is conserved to regulate mtDNA biogenesis. **a**, qRT-PCR analysis of *egl-20* in TGW, TQG and WT animals. n=8 independent experiments. **b, c**, Fluorescence visualization of the *hsp-6p::gfp*(**b**) and fold change in relative mtDNA levels (**c**) in TQG, TQG; *egl-20*(-/-) animals. n=4 independent experiments. **d-f**, Representative immunoblots (**d**) and quantifications (**e, f**) of mitochondrial OXPHOS proteins in *egl-20*(-/-) and TQG; *egl-20*(-/-) animals. n=3 independent experiments. **g, h**, Fluorescence visualization (**g**) and quantifications (**h**) of the *hsp-6p::gfp* reporter in TGW (n=32 worms), TGW; *vps-35*(-/-) (n=30 worms) and TGW; *vps-35*(+/+) (n=30 worms) animals. **i**, Fold change in mtDNA/nDNA ratios of animals shown in (**g**). n=4 independent experiments. **j, k**, Fluorescence visualization (**j**) and quantifications (**k**) of the *hsp-6p::gfp* reporter in TGW (n=31 worms), TGW; *mig-14*(-/-) (n=30 worms) and TGW; *mig-14*(+/+) (n=31 worms). **l**, Fold change in mtDNA/nDNA ratios of animals shown in (**j**). n=4 independent experiments. **m, n**, Fluorescence visualization (**m**) and quantifications (**n**) of the *hsp-6p::gfp* reporter in TGW animals in different mutant background. WT n=35 worms, *cwn-1* n=35 worms, *cwn-2* n=29 worms, *lin-44* n=34 worms, *lin-17* n=29 worms, *mig-1* n=30 worms. **o**, Fold change in mtDNA/nDNA ratios of animals shown in **m**. n=3 independent experiments. **p**, Fluorescence visualization of the *hsp-6p::gfp* reporter in TGW animals treated with EV or *bar-1* RNAi. Data shown represent three independent experiments with similar results. **q, r**, Fold change in mtDNA/nDNA ratios of TGW and WT animals treated with EV or *bar-1* RNAi that since oogenesis (**q**, n=6 independent experiments) and zygotically development (**r**, n=5 independent experiments). **s, t**, Wnt target gene *axin2* transcripts (**s**) and β -catenin protein level (**t**) in HEK293T cells treated with different concentrations of CHIR-99021 for 6 h. n=3 independent experiments. **u, v**, Wnt target gene *axin2* transcripts (**u**) and β -catenin protein level (**v**) in HEK293T cells treated with 10 μ M CHIR-99021 at different time points. n=4 independent experiments. Scale bars, 250 μ m. Data are the mean \pm s.e.m., ***P<0.001, **P<0.01, *P<0.05, ns denotes P>0.05, P values were determined using two-way ANOVA (**q, r**), one-way ANOVA (**a, c, h, l, k, l, n, o, s, u**) and two-sided Student's t-test (**e, f, w, x**). The exact P values are provided in Source Data Extended Data Fig. 6. Statistics source data and unprocessed western blots are provided.



Extended Data Fig. 7 | Distribution of SNPs and indels of genome for ED3011 and KR314. **a**, Circos-plot of mitochondrial genome features of ED3011 and KR314. The circles from the inside going in represent the *C. elegans* mitochondrial genome, nucleotide variations of KR314 and ED3011 (as the black line indicated) compared to N2. The circles on the outside represent the gene names on the mtDNA. **b**, Circos-plot of nuclear genome features of ED3011 and KR314. Segmented circles on the inside represent the six *C. elegans* chromosomes. Track 1, 2, 3, 4 are the histograms represent the numbers of variations per 10 kb (outward pointing bars = higher density.), Track 1 shows the SNPs of ED3011. Track 2 shows the SNPs of KR314. Track 3 represents the indels of ED3011. Track 4 represents the indels of KR314. Track 5 is the heatmap depicts the density of CDS (dark red = higher density) on *C. elegans* chromosomes. Circos graph were generated with the basic information of *C. elegans* genome WBcel235 (BioProject PRJNA13758) using TBtools⁶¹. See Supplementary Table 5 for the list of genetic variations identified in wild *C. elegans* strain ED3011 and KR314.



Extended Data Fig. 8 | The transgenerational induction of the UPR^{mt} provides benefits to offspring under stress conditions. **a-d**, Lifespan analysis of TGW and TGQ animals compared to WT animals. **e-h**, PA14 slow killing assay of TGW and TGQ animals compared to WT animals. **i**, Survival rates of day 1 adult WT and TGQ animals after paraquat treatment. $n=4$ independent experiments. **j**, Survival rates of D1 adult WT and TGQ animals after heat shock treatment. $n=5$ independent experiments. **k**, Lifespan analysis of N2 and other wild *C. elegans* strains ED3011 and KR314. **l-o**, Lifespan analysis of TGQ and TGW animals in *polg-1(tm2685)* (**l**), *fzo-1(tm1133)* (**m**), *atfs-1(gk3094)* (**n**) and *egl-20(n585)* (**o**) background. Data are the mean \pm s.e.m., *** $P < 0.001$, ** $P < 0.01$, P values were determined using two-sided Student's *t*-test (**i, j**). The exact P values are provided in Source Data Extended Data Fig. 8. Statistics source data are provided.

Corresponding author(s): Ye Tian

Last updated by author(s): May 8, 2021

Reporting Summary

Nature Research wishes to improve the reproducibility of the work that we publish. This form provides structure for consistency and transparency in reporting. For further information on Nature Research policies, see our [Editorial Policies](#) and the [Editorial Policy Checklist](#).

Statistics

For all statistical analyses, confirm that the following items are present in the figure legend, table legend, main text, or Methods section.

n/a Confirmed

- The exact sample size (n) for each experimental group/condition, given as a discrete number and unit of measurement
- A statement on whether measurements were taken from distinct samples or whether the same sample was measured repeatedly
- The statistical test(s) used AND whether they are one- or two-sided
Only common tests should be described solely by name; describe more complex techniques in the Methods section.
- A description of all covariates tested
- A description of any assumptions or corrections, such as tests of normality and adjustment for multiple comparisons
- A full description of the statistical parameters including central tendency (e.g. means) or other basic estimates (e.g. regression coefficient) AND variation (e.g. standard deviation) or associated estimates of uncertainty (e.g. confidence intervals)
- For null hypothesis testing, the test statistic (e.g. F , t , r) with confidence intervals, effect sizes, degrees of freedom and P value noted
Give P values as exact values whenever suitable.
- For Bayesian analysis, information on the choice of priors and Markov chain Monte Carlo settings
- For hierarchical and complex designs, identification of the appropriate level for tests and full reporting of outcomes
- Estimates of effect sizes (e.g. Cohen's d , Pearson's r), indicating how they were calculated

Our web collection on [statistics for biologists](#) contains articles on many of the points above.

Software and code

Policy information about [availability of computer code](#)

Data collection LAS X software 3.3.016799

Data analysis GraphPad Prism 6.01, ImageJ 1.48v, TBtools v1.082, TopHat v2.0.0, VCFtools 0.1.11, DESeq2 1.20.0

For manuscripts utilizing custom algorithms or software that are central to the research but not yet described in published literature, software must be made available to editors and reviewers. We strongly encourage code deposition in a community repository (e.g. GitHub). See the Nature Research [guidelines for submitting code & software](#) for further information.

Data

Policy information about [availability of data](#)

All manuscripts must include a [data availability statement](#). This statement should provide the following information, where applicable:

- Accession codes, unique identifiers, or web links for publicly available datasets
- A list of figures that have associated raw data
- A description of any restrictions on data availability

The accession number for the raw sequencing files and the processed data reported in this paper are NCBI GEO: GSE157031, NCBI BioProject: PRJNA607689 and NCBI BioProject: PRJNA727630. Previously published DNA sequence data that were used here are available under accession code PRJNA13758. Accessible link of KEGG pathway database used in this study is <http://www.genome.jp/kegg/>. All other data supporting the findings of this study are available from the corresponding author on reasonable request.

Field-specific reporting

Please select the one below that is the best fit for your research. If you are not sure, read the appropriate sections before making your selection.

Life sciences

Behavioural & social sciences

Ecological, evolutionary & environmental sciences

For a reference copy of the document with all sections, see nature.com/documents/nr-reporting-summary-flat.pdf

Life sciences study design

All studies must disclose on these points even when the disclosure is negative.

Sample size

No statistical method was used to predetermine sample size. For each experiment the n values were reported in the legend. For the fluorescences quantification, about 30 worms were analyzed based on our previous experience with the experimental model and techniques, the sample size of 30 worms provides robust statistical power for analysis. For RNAseq and DNAseq, synchronous population of 10,000 worms were used at the developmental time point of 48 hours post hatching, this sample size were experimentally optimized in our lab to be sufficient to obtain large amount of RNAs or DNAs. For mtDNA measurement, 30 early L4 (unless otherwise stated) worms were used, as was mentioned in the reference (PMID: 27135930). For the lifespan assay, 100–300 worms were analyzed based on published literature (PMID: 12471266). Sample size of the brood size experiments was determined according to the published literature (PMID: 32015436) using at least 10 worms for each strain.

Data exclusions

In general, data were not excluded. For lifespan and survival assay, worms that crawled off the plate, exploded or bagged were not included in the data (pre-established criteria). This exclusion criteria is extensively used in the field.

Replication

All experiments were performed at least three times yielding similar results and comprised of biological replicates.

Randomization

Randomization was not used and relevant to this study. For all experiments worms were grouped according to genotype. For all experiments cells were grouped according to different drug or siRNA treatment.

Blinding

Investigators were blinded in mtDNA measurement, lifespan analysis and stress resistance analysis of wild type and trans worms. In other cases, the experiment were not done blindly as the genotypes or the treatment effects are identifiable by visible traits.

Reporting for specific materials, systems and methods

We require information from authors about some types of materials, experimental systems and methods used in many studies. Here, indicate whether each material, system or method listed is relevant to your study. If you are not sure if a list item applies to your research, read the appropriate section before selecting a response.

Materials & experimental systems

n/a	Involved in the study
<input type="checkbox"/>	<input checked="" type="checkbox"/> Antibodies
<input type="checkbox"/>	<input checked="" type="checkbox"/> Eukaryotic cell lines
<input checked="" type="checkbox"/>	<input type="checkbox"/> Palaeontology and archaeology
<input type="checkbox"/>	<input checked="" type="checkbox"/> Animals and other organisms
<input checked="" type="checkbox"/>	<input type="checkbox"/> Human research participants
<input checked="" type="checkbox"/>	<input type="checkbox"/> Clinical data
<input checked="" type="checkbox"/>	<input type="checkbox"/> Dual use research of concern

Methods

n/a	Involved in the study
<input checked="" type="checkbox"/>	<input type="checkbox"/> ChIP-seq
<input checked="" type="checkbox"/>	<input type="checkbox"/> Flow cytometry
<input checked="" type="checkbox"/>	<input type="checkbox"/> MRI-based neuroimaging

Antibodies

Antibodies used

anti-GFP antibody (Santa Cruz Biotechnology sc-9996) (1:1000)
 anti-Tubulin antibody (Sigma T6074) (1:5000)
 anti-ATP5A (Abcam ab14748) (1:2000)
 anti-NDUFS3 (Abcam ab14711) (1:1000)
 anti-MTCO1/COX1 (Abcam ab14705) (1:500)
 anti-β-Catenin (BD 610154, dilution: 1:1000)
 anti-mouse secondary antibody (EarthOx E030110) (1/5000)

Validation

Well characterized antibodies were used in this study. All are commercially available and validated by the manufacturers.
 target, host, detail link
 anti-GFP, mouse, <https://www.scbt.com/zh/p/gfp-antibody-b-2;jsessionid=o9IU6tgUuEXPH1k4JhHdQ92zIEJ7r5iH6nirYONzne-pQtxoCn2j!1129980025>
 anti-Tubulin, mouse, <https://www.sigmaldrich.cn/CN/zh/product/sigma/t6074?context=product>
 anti-ATP5A, mouse, <https://www.abcam.cn/atp5a-antibody-15h4c4-mitochondrial-marker-ab14748.html>
 anti-NDUFS3, mouse, <https://www.abcam.cn/ndufs3-antibody-17d95-ab14711.html>

anti-MTCO1/COX1, mouse, <https://www.abcam.cn/mtnco1-antibody-1d6e1a8-ab14705.html>
 anti- β -Catenin, mouse, <https://www.bdbiosciences.com/cn/applications/research/stem-cell-research/cancer-research/human/purified-mouse-anti--catenin-14beta-catenin/p/610154>

Eukaryotic cell lines

Policy information about [cell lines](#)

Cell line source(s)	HEK293T (ATCC CRL-3216)
Authentication	The cell line was not authenticated.
Mycoplasma contamination	The cells tested negative for mycoplasma contamination
Commonly misidentified lines (See ICLAC register)	The study did not involve any commonly misidentified cell lines

Animals and other organisms

Policy information about [studies involving animals; ARRIVE guidelines](#) recommended for reporting animal research

Laboratory animals	Caenorhabditis elegans - N2 Bristol strain. SJ4100 (zcls13[hsp-6p::gfp] V) strain as wild-type (WT) AGD785 (rmls110[rgef-1p::Q40::yfp]; zcls13[hsp-6p::gfp] V) LTY43 (ythls3[rgef-1p::egl-20 + myo-2p::tdTomato]; zcls13[hsp-6p::gfp]) LTY44 (ythls4[rgef-1p::egl-20 + myo-2p::tdTomato]; zcls13[hsp-6p::gfp]) VC1390 (vps-35(ok1880) II) EW12 (mig-14(ga62) II) MT1215 (egl-20(n585) IV) VC3201 (atfs-1(gk3094) V) MT13232 (lin-65(n3441) I) RB763 (cwn-1(ok546) II) VC636 (cwn-2(ok895) IV) MT5383 (lin-44(n1792) I) VC1024 (pdr-1(gk448) III) RB2547 (pink-1(ok3538) II) CU6372 (drp-1(tm1108) IV) CU5991 (fzo-1(tm1133) II) BLW1632 (polg-1(tm2685)/mln1 [dpy-10(e128) mls14] II) AGD1617 (vps-35(ok1880) II; zcls13[hsp-6p::gfp]) LTY93 (mig-14(ga62) II; zcls13[hsp-6p::gfp]) AGD1618 (egl-20(n585) IV; zcls13[hsp-6p::gfp]) LTY408 (atfs-1(gk3094) V; zcls13[hsp-6p::gfp]) AGD1294 (lin-65(n3441) I; zcls13[hsp-6p::gfp]) LTY1001 (cwn-1(ok546) II; zcls13[hsp-6p::gfp]) LTY1002 (cwn-2(ok895) IV; zcls13[hsp-6p::gfp]) LTY1000 (lin-44(n1792) I; zcls13[hsp-6p::gfp]) LTY92 (mig-1(e1787) I; zcls13[hsp-6p::gfp]) LTY998 (lin-17(sy277) I; zcls13[hsp-6p::gfp]) LTY999 (tph-1(mg280) II; zcls13[hsp-6p::gfp]) LTY987 (TGW1; zcls13[hsp-6p::gfp]) LTY988 (TGW2; zcls13[hsp-6p::gfp]) LTY989 (TGW3; zcls13[hsp-6p::gfp]) LTY1388 (TGW4; zcls13[hsp-6p::gfp]) LTY1043 (TGW1; zcls13[hsp-6p::gfp]) LTY1387 (TGW2; zcls13[hsp-6p::gfp]) LTY958 (TGW2; vps-35(ok1880) II; zcls13[hsp-6p::gfp]) LTY960 (TGW2; mig-14(ga62) II; zcls13[hsp-6p::gfp]) LTY957 (TGW3; egl-20(n585) IV; zcls13[hsp-6p::gfp]) LTY959 (TGW3; atfs-1(gk3094) V; zcls13[hsp-6p::gfp]) LTY1062 (TGW3; lin-65(n3441) I; zcls13[hsp-6p::gfp]) LTY1058 (TGW3; cwn-1(ok546) II; zcls13[hsp-6p::gfp]) LTY1060 (TGW3; cwn-2(ok895) IV; zcls13[hsp-6p::gfp]) LTY1056 (TGW3; lin-44(n1792) I; zcls13[hsp-6p::gfp]) LTY1054 (TGW3; mig-1(e1787) I; zcls13[hsp-6p::gfp]) LTY1050 (TGW3; lin-17(sy277) I; zcls13[hsp-6p::gfp]) LTY1052 (TGW3; tph-1(mg280) II; zcls13[hsp-6p::gfp]) SJZ47 (foxSi16[myo-3p::tomm-20::mKate2::HA::tbb-2 3' UTR] I.) SJZ204 (foxSi37[ges-1p::tomm-20::mKate2::HA::tbb-2 3' UTR] I.) SJZ106 (foxSi27[pie-1p::tomm-20::mKate2::HA::tbb-2 3' UTR] I.) LTY954 (zcls13[hsp-6p::gfp]; foxSi16[myo-3p::tomm-20::mKate2::HA::tbb-2 3' UTR] I.) LTY1043 (TGW1; zcls13[hsp-6p::gfp]; foxSi16[myo-3p::tomm-20::mKate2::HA::tbb-2 3' UTR] I.) LTY1065 (pdr-1(gk448) III; zcls13[hsp-6p::gfp])
--------------------	---

LTY1066 (pdrl-1(gk448) III; ythls3[rgef-1p::egl-20 + myo-2p::tdTomato]; zcls13[hsp-6p::gfp])
LTY1093 (pink-1(ok3539) II; zcls13[hsp-6p::gfp])
LTY1094 (pink-1(ok3539) II; ythls3[rgef-1p::egl-20 + myo-2p::tdTomato]; zcls13[hsp-6p::gfp])
LTY168 (drp-1(tm1108) IV; zcls13[hsp-6p::gfp])
LTY1558 (drp-1(tm1108) IV; TGW1; zcls13[hsp-6p::gfp])
LTY1559 (drp-1(tm1108) IV; TGQ1; zcls13[hsp-6p::gfp])
LTY160 (fzo-1(tm1133) II; zcls13[hsp-6p::gfp])
LTY1555 (fzo-1(tm1133) II; TGW1; zcls13[hsp-6p::gfp])
LTY1556 (fzo-1(tm1133) II; TGQ1; zcls13[hsp-6p::gfp])
LTY1391 (TGQ1; egl-20(n585) IV; zcls13[hsp-6p::gfp])
LTY1389 (TGQ1; atfs-1(gk3094) V; zcls13[hsp-6p::gfp])
LTY160 (polg-1(tm2685)/mln1 [dpy-10(e128) mls14] II; zcls13[hsp-6p::gfp])
LTY1555 (polg-1(tm2685)/mln1 [dpy-10(e128) mls14] II; TGW1; zcls13[hsp-6p::gfp])
LTY1556 (polg-1(tm2685)/mln1 [dpy-10(e128) mls14] II; TGQ1; zcls13[hsp-6p::gfp])
AB1
AB3
CB4854
CB4855
CB4856
CB4857
CB4932
CX11262
CX11285
ED3011
ED3017
ED3040
ED3052
EG4725
JT11398
JU1088
JU258
JU360
MY1
MY14
RC301
CB4852
KR314

Wild animals

No wild animals were used in this study

Field-collected samples

No field collections were used in this study.

Ethics oversight

No ethical approval or guidance required.

Note that full information on the approval of the study protocol must also be provided in the manuscript.